CHALMERS
UNIVERSITY OF TECHNOLOGY

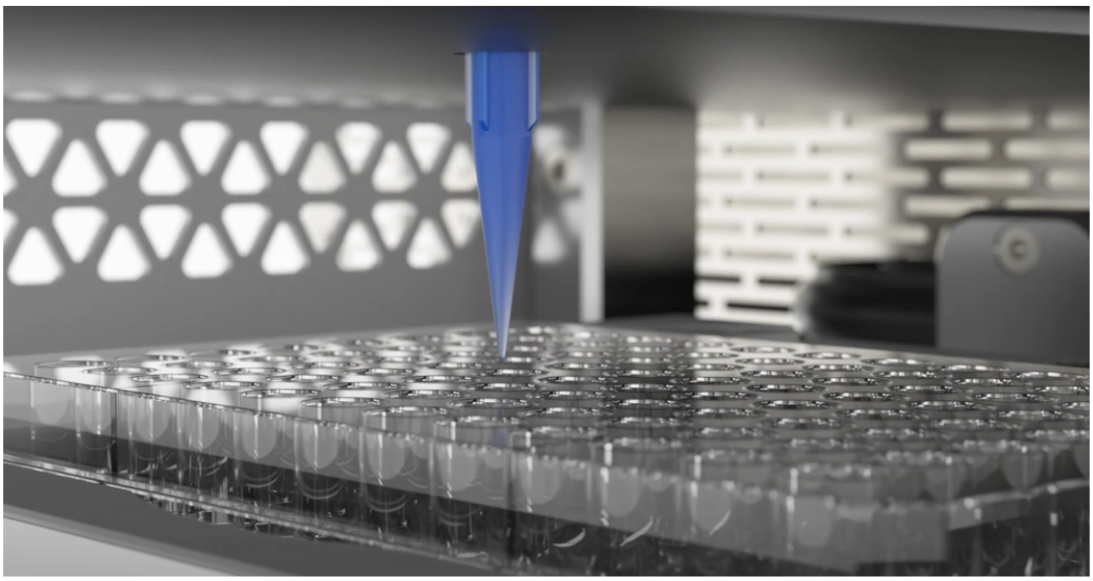

Advancing in vitro models for high-throughput 3D bioprinting

Comprehensive validation and optimization of an advanced automated 3D bioprinter

Master's thesis in Master Materials Engineering

LAIA MOLINER CARRILLO

INDUSTRIAL AND MATERIALS SCIENCE

CHALMERS UNIVERSITY OF TECHNOLOGY
Gothenburg, Sweden 2024
www.chalmers.se

Master's thesis 2024

Advancing in vitro models for high-throughput 3D bioprinting

Comprehensive validation and optimization of an advanced automated 3D bioprinter

LAIA MOLINER CARRILLO

CHALMERS
UNIVERSITY OF TECHNOLOGY

Industrial and Materials Science
Materials and Manufacture
CELLINK AB
Chalmers University of Technology
Gothenburg, Sweden 2024

Advancing in vitro models for high-throughput 3D bioprinting
Comprehensive validation and optimization of an advanced automated 3D bioprinter
LAIA MOLINER CARRILLO

Supervisor: Dr. Paulo Godoy, CELLINK
Examiner: Dr. Uta Klement, Industrial and Materials Science

Master's Thesis 2024
Industrial and Materials Science
Materials and Manufacture
CELLINK AB
Chalmers University of Technology
SE-412 96 Gothenburg
Telephone +46 31 772 1000

Cover: Reconstruction of droplet dispensing using a conical nozzle inside the BIO CELLX. Image from CELLINK, used with the permission of the author. Typeset in LaTeX
Printed by Chalmers Reproservice
Gothenburg, Sweden 2024

Advancing in vitro models for high-throughput 3D bioprinting
Comprehensive validation and optimization of an advanced automated 3D bioprinter
LAIA MOLINER CARRILLO
Industrial and Materials Science
Chalmers University of Technology

Abstract

Three-dimensional in vitro models have been proposed as a solution to reduce the high failure rates in clinical trials. Even so, there is a clear lack of techniques capable of creating these cell culture models in a straightforward, cost-effective, and rapid manner, enabling researchers and companies to perform large-scale screenings. One promising candidate to address this need is three-dimensional bioprinting, a technology that can generate viable constructs using biomaterials, cells, and biological molecules. In this context, CELLINK has developed the BIO CELLX biodispenser, which combines liquid dispensing and bioprinting in a highly automated system, significantly reducing human intervention. Despite its potential, it remains uncertain whether this technology can effectively accelerate the laborious processes currently associated with preclinical stages. This study evaluates the key factors necessary for the implementation of BIO CELLX as a high-throughput bioprinter and explores workflow optimizations that could enhance both the dispensing process and the resulting outcomes. The workflow has been validated for new software release and hardware modifications to achieve full functionality, demonstrating high droplet accuracy and uniform mixing. Results indicate that increasing the number of mixing cycles does not negatively impact cell viability; on the contrary, it enhances homogeneous cell density and overall cell viability. Additionally, the performed experiments suggest that the usage of nozzles with larger diameters, along with adapted dispensing parameters, can improve droplet centralization. This project provides an in-depth analysis, highlighting crucial elements required to achieve a precise and efficient three-dimensional bioprinter.

Keywords: Three-dimensional bioprinting, 3D in vitro models, high-throughput screening, BIO CELLX biodispenser, dispensing parameters

Acknowledgements

I would like to extend my deepest gratitude to my examiner, Dr. Uta Klement, for her constant support and guidance throughout this process. Her assistance and encouragement have been invaluable to the completion of this thesis.

I am also profoundly grateful to CELLINK for providing me with the opportunity to conduct this thesis. Special thanks to the Science and Application Department, as well as the Hardware and Software teams. They have made me feel welcome from the very first moment and have provided me with incredible advice that I will carry with me not only for this work but throughout my future career. Without their expertise and assistance, this experience would not have been the same.

Moreover, I would like to express a deep thanks to my family, especially my mom, for being my biggest support during this master's journey. Their support and belief in me have been my pillar of strength.

To my friends, thank you for cheering me on during the tough times and celebrating with me during the high moments. Your encouragement and companionship have made this journey all the more enjoyable.

Lastly, but by no means least, I want to express my heartfelt thanks to Dr. Paulo Godoy. His eternal patience and magnificent support have been the backbone of this work. He has been an amazing supervisor, and from him, I have not only gained immense knowledge but also learned about the passion that this field requires. For this, I am eternally grateful.

Laia Moliner Carrillo, Gothenburg, June 2024

List of Acronyms

Below is the list of acronyms that have been used throughout this thesis listed in alphabetical order:

2D	Two-Dimensional
3D	Three-Dimensional
ABL	Automatic Bed Leveling
AM	Additive Manufacturing
ANOVA	Analysis of Variance
ATCC	American Culture Collection
AU	Arbitrary Units
CV	Coefficient of Variance
DAPI	4',6-Diamidino-2-Phenylindole
DMEM	Dulbecco's Modified Eagle Medium
ECM	Extracellular Matrix
FBS	Fetal Bovine Serum
FITC	Fluorescein Isothiocyanate
HBSS	Hanks' Balanced Salt Solution
HEPA	High-Efficiency Particulate Air
hTERT	Human Telomerase Reverse Transcriptase
HTS	High-Throughput Screening
IPA	Isopropyl Alcohol
IPv4	Internet Protocol Version 4
LAF	Laminar Airflow
MSCs	Mesenchymal Stem Cells
PBS	Phosphate-Buffered Saline
Pen-Strep	Penicillin-Streptomycin
SD	Standard Deviation
TIFF	Tag Image File Format
TRS	Technical Requirement Specifications
TXRED	Texas Red
UV	Ultraviolet

Nomenclature

Below is the nomenclature of parameters and variables that have been used throughout this thesis.

Parameters

N_0	Initial number of cells at the beginning of the incubation time

Variables

T_d	Doubling time
t	Time
N_t	Number of cells at the end of the incubation time

Contents

List of Figures

List of Tables

1
Introduction

Three-dimensional (3D) bioprinting is an emerging field with significant applications in tissue engineering and medicine [1]. *In vitro* models created through 3D bioprinting offer precise control over cell populations, extracellular matrix (ECM) deposition, dynamic microenvironments, and sophisticated microarchitecture [2]. These models are crucial for drug screening, reducing the need for costly *in vivo* experiments, and accelerating new drug development [3]. High-throughput 3D bioprinting is particularly valuable as it allows for the screening of large chemical libraries against various molecular targets, enabling Pharma and Biotech companies to test and discover key compounds for diseases like cancer more efficiently [4].

The BIO CELLX biodispenser, developed by CELLINK, combines liquid dispensing and bioprinting, automating critical tasks such as reagent mixing, cell integration with bioink, maintaining a sterile environment, and automatic wiping and priming. Before deploying the BIO CELLX biodispenser to new users, thorough evaluation and validation of workflows and new features are essential to ensure the system meets the highest standards for successful research and experimentation. Achieving high throughput with BIO CELLX requires extensive dispensing validations and cell viability tests to assess its practical application.

1.1 Aim

The aim of this study is to investigate the feasibility of conducting high-throughput *in vitro* models using the biodispenser developed by CELLINK, named BIO CELLX. For this purpose, an examination and validation of the technical printing capabilities were conducted, along with cellular studies. This aims to guarantee efficient dispensing that meets the demands of high-throughput processes while optimizing cell viability.

In this research, the feasibility of droplet dispensing into a 384-well plate without contacting the well walls or experiencing significant evaporation was explored. Additionally, an evaluation was performed to validate the use of needle dispensing to increase printing precision without adversely affecting cell survival. During this study, new software releases were thoroughly tested to identify any usability issues or errors.

To ensure that the *in vitro* models dispensed mimic real conditions as closely as

possible, cell cultures under sterile conditions were conducted, monitoring cellular doubling time, viability, and morphology before and after printing. Moreover, the mixing setup in the collagen droplet dispensing workflow was refined to enhance the efficiency of cell and bioink mixing and prevent cell damage.

1.2 Research questions

The ultimate objective of this study is to answer the following questions formulated:

1. How should dispensing parameters be changed to achieve precise droplets in a 384 well-plate without touching well walls or be exposed to meaningful heterogeneous evaporation?
2. How do cells react when an increased number of mixing cycles are conducted?
3. How do cells react when a cylindrical nozzle is used for dispensing compared to a conical nozzle?

Together with the aforementioned questions, the thesis should help to validate and encounter any issue related to new software release or hardware modification conducted during the realization of the work.

1.3 Limitations

The major limitation of this research is the system novelty, thus integrating new features necessitates adjustments for both hardware and software. Achieving full functionality takes time, and rigorous testing is essential before validation.

Another point that needs to be considered is the uncertainties that the desired low volume range introduces. Determining optimal parameters for cell viability while maintaining precise mixing remains a challenge. Therefore, changes in dispensing parameters required to be validated, given that minor modifications could potentially impact cell survival.

2
Theory

In the following section the most relevant information to effectively comprehend the content of the project is explained.

2.1 2D vs 3D *in vitro* models

Nowadays, successful outcomes during clinical trials remain a challenge in the healthcare industry [5]. This issue largely arises from the poor connection between preclinical results obtained using *in vitro* methodologies and the *in vivo* data from clinical trials. One key factor to consider when addressing these discrepancies is the widespread use of two-dimensional (2D) cell culture models in *in vitro* experiments [6, 7]. Although 2D cell models have played a crucial role in research since 1900, several studies have highlighted their limitations in accurately mimicking *in vivo* tissue cells [7, 8].

Even though 2D models are known to lack the tissue complexity and the essential cell-to-cell and cell-to-ECM interactions that 3D architecture possesses, they offer significant advantages that should not be overlooked. These include being a well-established method that allows easy cell observation and measurements, cost-effectiveness, and rapid workflows [6, 9].

To bridge the gap between preclinical and clinical stages, 3D cell models have been postulated as promising candidates. These models offer a more reliable transition from *in vitro* to *in vivo* trials, potentially reducing the failure rate and shortening the testing process for new molecules [10]. Some of the latest innovative strategies for achieving functional 3D cell cultures in the laboratory include microfluidic systems, the hanging drop method, or the rapidly increasing area of 3D bioprinting [11].

Table 2.1 compares key biological features of both *in vitro* models to give a brief insight into the main differences between the two methods [5, 7, 12, 13].

2.2 3D bioprinting

Additive manufacturing (AM), also known as 3D printing, creates 3D constructs by adding material layer by layer [14]. 3D bioprinting, a subset of AM, specifically generates structures using viable cells, biomaterials, and biological molecules. To ensure the viability of these constructs, it is crucial to maintain cell viability during

Table 2.1: Biological comparison of 2D and 3D cell cultures.

Features	**2D Cell Culture**	**3D Cell Culture**
Cell morphology	Unnatural cell shape characterized by flat and elongated morphology in a mono layer	Natural shape forming 3D clusters with several layers
Nutrients exposure	All the cells are exposed to the same amount of medium, receiving similar quantities of nutrients	Cells are differently exposed to cell medium being the inner layers often lacking some nutrients as oxygen due to the low penetration of the solution
Cell proliferation	Growth rate is unnaturally fast	The cells growth vary depending on the cell type and the technique used
Cell interaction	Interactions between cells in culture are rarely observed and not realistic	Allow communication between the cell and the matrix and between adjacent cells
Gene and protein expression	Gene and protein expression profiles are extremely different compared to *in vivo* cases	Gene and protein expression profiles are similar compared to *in vivo* models

and after the manufacturing process, promote cell growth, and provide mechanical stability [15]. Although 3D bioprinting originated in tissue engineering to replicate organs, it has applications in other areas such as cell-based sensors, drug and toxicity screenings, and tissue and tumor models [16]. Different methods have been developed to create constructs suitable for these various fields.

Firstly, droplet-based bioprinting generates small droplets that can be aggregated to form 3D models. Different techniques produce these droplets. For instance, inkjet bioprinting utilizes the physical properties of bioinks (e.g., viscosity, surface tension, and density) to deposit microspheres onto a substrate. Electrohydrodynamic jetting employs an electric field to control droplet formation, while laser-assisted bioprinting uses laser guidance to precisely place droplets.

Secondly, light-based bioprinting solidifies photosensitive polymers with controlled light exposure to create highly detailed constructs. Different techniques within this modality are based on the type of light scanning mode used [17].

Lastly, extrusion-based bioprinting is the most widely used method due to its compatibility with various biomaterials and low cost. It involves extruding bioinks through a nozzle to build structures layer by layer [17, 18].

Despite the precision, fast printing, and low cost of droplet-based and light-based bioprinting, extrusion-based bioprinting remains the most common due to its compatibility with various biomaterials and low cost [17, 18].

2.2.1 Extrusion-based bioprinting

Extrusion-based bioprinting, also known as pressure-assisted bioprinting, relies on the extrusion of a selected bioink through one or more nozzle orifices by applying pressure. This pressure can be generated by pneumatic, plunger, or screw-based systems, coordinating to produce a continuous filament for layer-by-layer deposition [18]. This method is capable of printing simple shapes, such as droplets, to complex 3D structures. The popularity of this technique can be attributed to its ability to work with a wide range of bioink viscosities and to fabricate designs with high cell densities, reaching up to more than one million cells per milliliter [19]. Nevertheless, there are limitations that need to be considered, such as limited resolution, time consumption, and potential cell damage due to the shear stress generated during bioprinting [19, 20].

To try to overcome these challenges, maintaining precise control during the printing process is essential for achieving accurate results, particularly when aiming to increase the precision of the print or to decrease the time of the process [21]. This control encompasses not only printing movements such as extrusion rate and volume but also key variables like retraction, z-offset position, and travel speed. The z-offset position, which is the distance between the nozzle tip and the print bed in the z-axis, is critical for ensuring proper adhesion of the print to the substrate. In the case of retraction, defined as a counter-clockwise movement (with extrusion being clockwise), it is crucial for preventing oozing during non-printing movements [22, 21]. Retraction is characterized by its length (or distance) and speed. Consequently, these parameters are vital for ensuring printing quality, avoiding irregularities, and reducing printing time [21].

2.2.1.1 High throughput bioprinting

Nowadays, many pharmaceutical and biological research fields demand high-throughput technologies to create 3D cell models. These technologies would allow, for instance, the testing of chemical compounds in biological systems using high-throughput screening (HTS) [23, 24]. However, most of the equipment developed so far is designed for large-scale 2D cell culture experiments, which are not reliable when results are compared to *in vivo* testing [23]. Nevertheless, the requirements to operate in high-throughput are not easy to meet, as they necessitate the use of 384-well plates or greater, and criteria such as having outliers less than 2% of the total and a coefficient of variation (CV) between the samples not greater than 20% [23, 25]. Achieving these requirements for 3D bioprinting technologies, especially extrusion-based ones due to their low cost and high flexibility, would be a significant innovative step. However, challenges such as the speed of printing and resolution have been encountered. Therefore, companies are attempting to develop new products that can overcome these challenges and meet these tough requirements [23].

2.2.1.2 BIO CELLX

In order to adapt to customer needs, CELLINK is developing a new bioprinter prototype that is able to present a cost-effective and time-efficient automated 3D cell culture workflow. To achieve these key factors, six cornerstones are planned to be achieved (see Fig. 2.1) [26]:

- A highly precise positive displacement extrusion system that can achieve reproducible results across samples.
- Enclosure that maintains sterility thanks to a high-efficiency particulate air (HEPA) filter.
- Ready-to-use protocols with validated pre-set dispensing parameters that ensure accurate results.
- Automated calibration using a sensor that measures the position of each nozzle outlet in relation to the position of the vessel. Moreover, an algorithm compensates for any possible inaccuracy to ensure precise positioning of the dispensed model.
- A workflow that ensures maximized cell viability, creating highly functional cellular models.
- Automated mixing of bioinks, reagents, and cell suspension, achieving homogeneous cell density and reducing variation between samples and the time required for human-intensive tasks.

To achieve these objectives, BIO CELLX presents a comprehensive workflow. First, a preparation stage is required, in which cells need to be cultured and expanded, and a bioink needs to be selected (currently, only offering TeloCol as a validated protocol). Then, the dispensing protocol begins, where the dispensing parameters are selected and the cells, bioink, and reagent are added to the material unit (see Fig. 2.2). In this unit, automatic mixing takes place thanks to a system of channels that connects each chamber, with pneumatic pressure applied in the bioink chamber and mechanical pressure due to a piston in the extrusion chamber. Next, the vessel is attached to the printbed, and the dispensing process takes place (see Fig. 2.1). Afterwards, thermal or photocrosslinking is conducted, and the constructs are ready to be collected. The user can then start their own analysis by adding cell medium and incubating the 3D *in vitro* models [26].

2.2.2 Bioinks

The capability of extrusion-based bioprinting to use a wide range of hydrogels is well known. However, not all the biomaterials employed can assure good resolution to mimic biological tissues or provide an adequate environment for cell survival and proliferation [17, 27]. For this reason, a tradeoff often needs to be made to obtain a functional print construct. Some biomaterials, such as glycol or alginate, possess favorable rheological and mechanical properties, such as adjustable viscosity, quick shear recovery, and shear thinning. These properties are extremely important to ensure good printability. For instance, if a material possesses high viscosity and shear-thinning properties, shape fidelity is guaranteed due to the viscosity, and

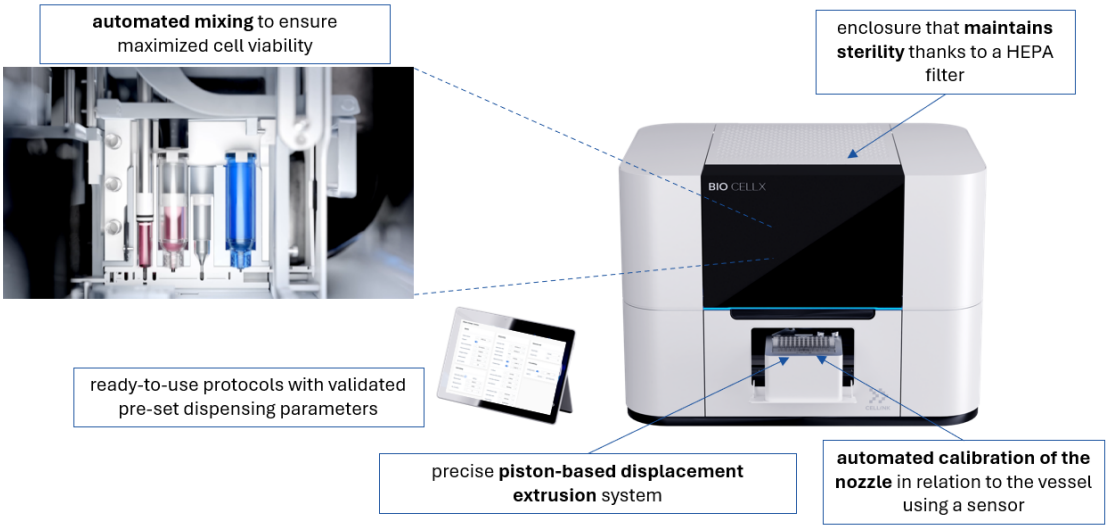

Figure 2.1: Image of the BIO CELLX bioprinter highlighting its main features. Printer images from CELLINK, used with the permission of the author.

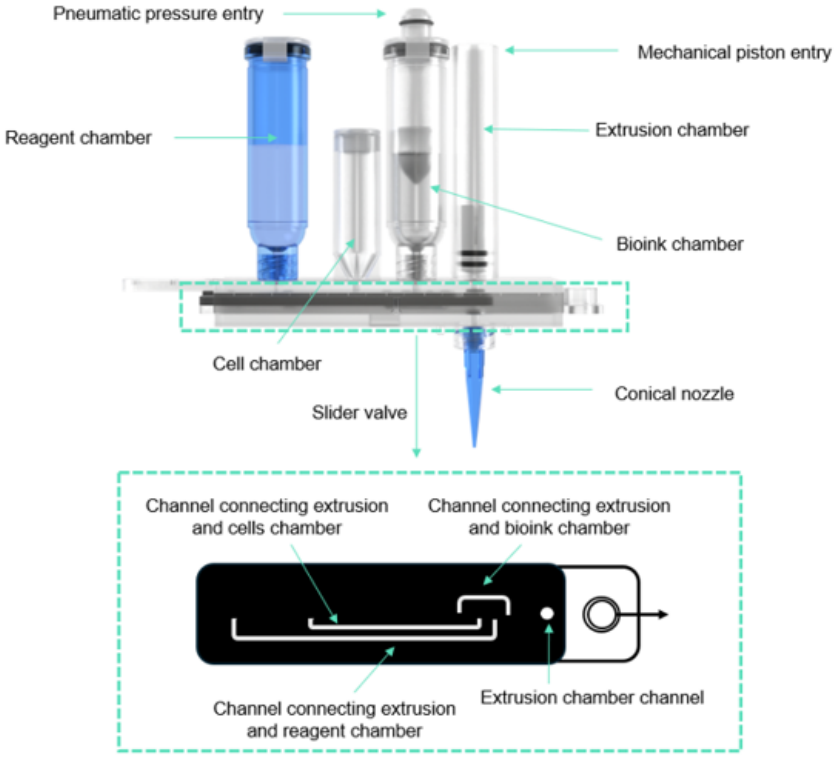

Figure 2.2: Diagram of the BIO CELLX material unit parts, detailing the components and their connections. The slider valve, which contains channels to connect the different chambers, changes position depending on the components being mixed at each moment. All mixed components are directed to the extrusion chamber where the piston applies pressure to extrude the mixed material through the conical nozzle. Printer images from CELLINK, used with the permission of the author.

shear thinning will reduce the stress needed to extrude the material through the nozzle by decreasing viscosity at increased shear rates, making this bioink ideal in terms of printability [27, 28, 29]. Nonetheless, these are not the only properties required for the selection of a bioink. Natural biomaterials such as collagen, gelatin, or chitosan exhibit more favorable biological properties compared to the first group. These biological properties can include biocompatibility, support of cell migration and proliferation, and cytocompatibility [27]. Therefore, the selection of the adequate bioink will highly depend on the final application. In the case of complex 3D constructs designed to mimic specific structures, rheological and mechanical properties are decisive to ensure good printability during the process. However, when simple shapes such as droplets are used to create *in vitro* models for drug testing, biological properties are the priority.

When selecting a biomaterial as bioink, its ability to crosslink is crucial. Hydrogels need gelation to maintain their shape after printing. There are two types of crosslinking: physical and chemical. Physical crosslinking is reversible and occurs due to polymer entanglement or ionic interactions. Chemical crosslinking, on the other hand, involves the formation of covalent bonds between components [30].

2.2.3 Collagen

Collagen is the most abundant protein in the human body and a major component of the ECM. Scientists use collagen to mimic the ECM in 3D *in vitro* models. As an endogenous component of the human body, collagen has unique properties such as cell recognition signals, the ability to form 3D constructs in various conformations, and controllable mechanical properties, making it a promising bioink [31]. Additionally, like many other protein-based hydrogels, collagen can undergo physical crosslinking, forming non-covalent bonds. This allows collagen fibers to form due to the folding of collagen proteins into hierarchical structures at neutral pH [32].

Collagen can be categorized into two types based on the extraction method: atelocollagen and telocollagen. Atelocollagen is obtained through enzyme extraction and lacks telopeptides. Telocollagen, on the other hand, is extracted with acid, maintaining the telopeptides intact. These telopeptides help collagen assemble into fibrils more easily, making telocollagen an efficient bioink [33, 34].

However, collagen is highly stable in acidic conditions, which is good for long-term storage but not ideal for immediate use as a bioink. Therefore, neutralizing the collagen with a NaOH solution is necessary to achieve a pH suitable for cell survival [35].

2.3 Cells

Since it is widely known that 3D *in vitro* cell cultures are more reliable for mimicking the reality of the body, it is logical that new treatments want to be tested with these types of models. For instance, using 3D bioprinting, 3D cell aggregates

of cancer cells, also called spheroids, could be dispensed and represent a helpful tool to precisely reproduce the 3D organization and microenvironmental factors of tumors [36]. Additionally, the use of mesenchymal stem cells (MSCs), multipotent adult stem cells that have the capacity to differentiate into several tissues, including cartilage, bone, fat, muscle, and others, could be useful to test the toxicity of some new drugs in specific healthy tissues [37, 38]. Therefore, all these cell types should be able to undergo the 3D bioprinting workflow without suffering any cell damage, ensuring that the workflow does not exert enough pressure to translate into shear stress that could have destructive effects on the cells [39].

3

Methods

This section presents the methods employed to validate the BIO CELLX workflow and optimize its dispensing parameters. Additionally, it details the cell culture study protocols used to assess cell viability and homogeneity with the same biodispenser.

3.1 Experimental overview

The methodology of this study is divided into three main sections, as illustrated in Figure 3.1: a) validation, b) optimization, and c) cell studies. Each task is essential for assessing if the new iteration of BIO CELLX displays the requirements neeeded to be considered a high-throughput biodispenser.

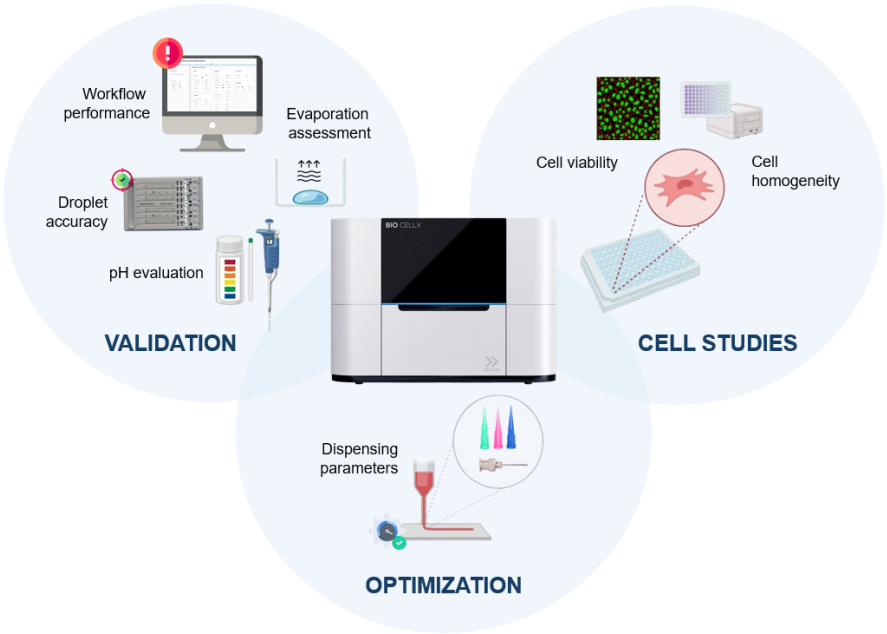

Figure 3.1: Diagram presenting the three main areas of focus in the study's methodology: validation, optimization, and cell studies.

To ensure the adequate functionality of the printer and to test its current capabilities, a comprehensive validation was conducted. This involved a thorough review of the printer workflow, documenting all incidences and reporting them to the software and hardware teams. Additionally, crucial factors to achieve a successful implementation

of 384-well plates were evaluated, including droplet accuracy, volume evaporation, and pH testing of the mixed solution.

After the finalization of this first step, the optimization of dispensing parameters started. These included the testing of various conical and cylindrical nozzles adjusting crucial settings such as extrusion rate or z-offset to ensure a precise and centralized printing, ultimately identifying the most optimal combination.

The final stage involved experiments with MSCs, to asses the mixing homogeneity and the cells survival during and after the dispensing process. To do so, cell viability and homogeneity assays were performed in different time points and under different mixing and dispensing conditions to find what could improve the quality of the print.

3.2 Validation

Achieving the successful printing of a well-plate, it is crucial that all stages of the process are perfectly executed. Therefore, several tests were conducted to evaluate the correct functionality of the overall dispensing workflow, as well as to assess key performance specifications such as droplet accuracy, evaporation rates, and pH levels.

3.2.1 Workflow performance

The user interface of BIO CELLX enables customers to follow a comprehensible workflow that concludes when all droplets are successfully dispensed and cross-linked in the well-plate. However, multiple software iterations are necessary to eliminate errors at all stages. To evaluate this, extensive tests of the overall procedure were conducted, reviewing specific aspects of each section. After each validation session, a report was compiled and sent to the software/hardware department, detailing each run, the issues encountered, and prioritizing them by severity.

3.2.1.1 System initialization

In the initial setup, the biodispenser was connected using Internet Protocol Version 4 (IPv4) and Ethernet for internet and network connections. The software version in use was documented, Ultraviolet (UV) sterilization was deactivated, and any previously installed material units were removed.

3.2.1.2 Settings configuration

At this stage, the type of vessel (6, 12, 24, 48, or 96-well plate) was selected along with the specific number of wells to be printed and the number of droplets per well. Next, the material was configured by selecting whether a new material unit or an existing mixed material unit was to be used. Subsequently, the TeloCol protocol was chosen, either 4 mg/mL or 6 mg/mL, and any modifications to the pre-set dispensing parameters were documented (see Fig. 3.2).

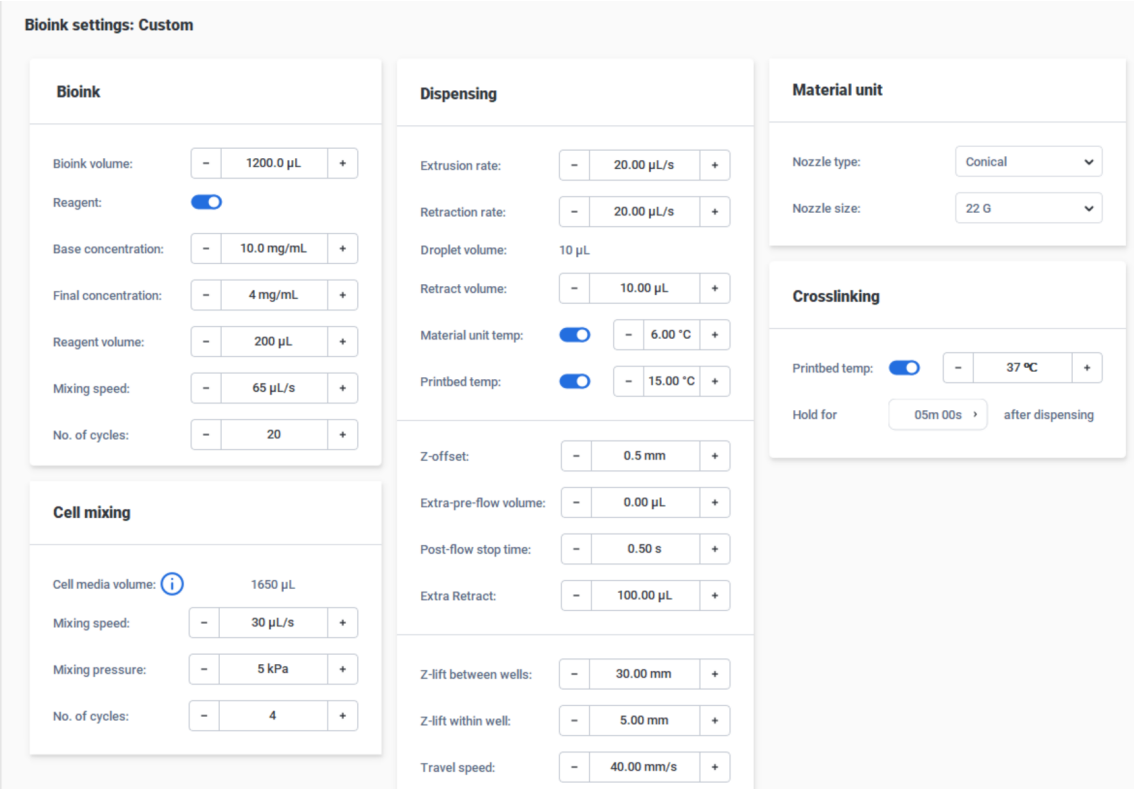

Figure 3.2: Material configuration screen of the BIO CELLX user interface displaying all the pre-set dispensing parameters.

3.2.1.3 Material unit and vessel loading

The material unit and TeloCol/alginate capsule (similar density to TeloCol and avoids the handling difficulties of thermal crosslinking) was assembled according to the guidelines described in Appendix A.1, and the material unit name was recorded. Before loading the material unit into the cartridge station, it was verified that the piston was in the upward position and the slider valve was successfully homed. Upon meeting these conditions, the material unit was loaded. The downward movement of the piston was then monitored to ensure proper mixing of the components inside the material unit. Finally, it was confirmed that the temperature in the cartridge station had reached the desired level, and the printbed hatch was opened to load the vessel.

3.2.1.4 Pre-dispensing preparation

During this phase, it was necessary to supervise the completion of all internal checks conducted by the printer. These included nozzle calibration, lid removal, and automatic bed leveling (ABL), along with ensuring that the printbed temperature reached its target. Once these steps were achieved, the nozzle needed to be primed. This involved verifying that the camera was functioning and that the nozzle was properly centered in view. Approximately 200 µL of reagent was then extruded, and the nozzle was wiped until no material residue was observed.

3.2.1.5 Dispensing and crosslinking

For this final step, it was essential to ensure that the camera was operational and that no material was attached to the nozzle before and during printing. During dispensing, it was observed that retraction, extrusion, and compensation were correctly performed, and that the temperature required for crosslinking was maintained. After the crosslinking process was completed, the vessel was detached, and the volume and centralization of the droplets were evaluated. Finally, the material unit used was cleaned for future uses following the cleaning guidelines in Appendix A.2.

3.2.2 Droplet accuracy

To evaluate the droplet accuracy of the BIO CELLX for volumes of 5 µL, 2.5 µL, and 1 µL, which are key for printing in small wells, a fast and quantitative capillary-based system called Checkit Go was used. In collaboration with the hardware department, Pronterface software was employed to control the printing process, allowing direct commands to be sent for printing in the wells of the Checkit Go plates.

The printer was loaded with 2 mL of Milli-Q water into the bioink chamber of the material unit. For the 5 µL and 2.5 µL droplets, 5 µL Checkit Go models with 8 channels and a useful range of 2.5 to 5 µL were used. A total of 96 droplets were measured for each condition, using 6 plates per condition and reusing each cartridge once. Additionally, for the 1 µL droplets, 4 droplets of 1 µL were printed in each well of the same 5 µL Checkit Go models, allowing the detection of inaccuracies for small volumes in this type of cartridge. Therefore, one cartridge was used, reusing it three times in total.

3.2.3 Evaporation assessment

Determining the degree of evaporation that occurs within the printer when dispensing small volumes is crucial for assessing the viability of these printings. Therefore, an experiment was conducted to measure the evaporation levels for 5 µL and 1 µL droplets. Before starting, the printer underwent a sterilization run. A 1.2 mL of 2% non-sterile alginate solution was then used as the bioink to mimic the density of TeloCol and avoid the crosslinking step. Moreover, 1.15 mL of water were utilized to simulate the reagent and cells components, an all was mixed using the pre-set dispensing parameters (see Fig. 3.2). Pronterface software was employed to dispense droplets into a 384-well plate. The well-plate was pre-weighed using a high-precision scale inside a laminar airflow (LAF) hood to prevent particle accumulation. Initially, 24 droplets of 5 µL were dispensed onto the plate. The plate was then weighed again and placed inside the printer for 50 minutes, simulating the duration required to print a complete 384-well plate. After this period, the well-plate was reweighed to evaluate the volume lost due to evaporation. This procedure was conducted five times for 8 µL and 8 times for 1 µL.

3.2.4 pH evaluation

To ensure that the mixing conducted by the printer creates a suitable environment for cell survival and proliferation, the pH level was evaluated. A material unit was prepared using 1.2 mL of non-sterile TeloCol (6 mg/mL) as the bioink, 0.5 mL of TeloCol neutralization solution, and 0.65 mL of Dulbecco's Modified Eagle Medium (DMEM) with 10% Fetal Bovine Serum (FBS) and 1% penicillin-streptomycin (Pen-Strep) and mixed with the printer. The pre-set values were selected (see Fig. 3.2), and 200 µL droplets were dispensed per well into a 24-well plate until no material remained.

Additionally, a control sample was prepared by hand mixing. For this, 0.3 mL of non-sterile TeloCol (6 mg/mL), 50 µL of TeloCol neutralization solution, and 0.15 mL of DMEM with 10% FBS and 1% Pen-Strep were used. The components were mixed by continuously transferring the mixture between two syringes equipped with Luer Locks, which were pre-cooled to prevent TeloCol crosslinking. This method aimed to ensure thorough mixing while minimizing bubble formation, stopping after 20 mixing cycles were conducted. From this hand-mixed preparation, 200 µL was dispensed into a well to serve as a control. Upon completion of all dispensing, two colorimetric tests were employed to determine the pH levels of the droplets: Duotest, with a useful range of pH 5 to 8, and Fisherbrand, with a useful range of pH 0 to 14. Small droplets were applied to the paper sticks using a 100 µL pipette, followed by a visual inspection to assess the pH.

3.3 Optimization

After addressing the overall workflow and various capabilities, the next step was to examine if the dispensing method could be optimized to improve the outcome. Consequently, the dispensing parameters were adjusted to find the most effective solution for enhancing aspects such as droplet centralization.

3.3.1 Dispensing parameters

Despite the existence of pre-set parameters, advancing to high-throughput printing demands extreme precision during all dispensing steps. This precision is necessary to achieve perfectly formed droplets that are dispensed in the center of the well. However, most droplets obtained with the pre-set parameters do not meet this standard since they were adapted using previous hardware and software versions, highlighting the need for optimization.

To address the optimization aspect, a systematic evaluation was conducted using the standard recommended 22G conical nozzle as the control, and comparing it with 20G and 18G sterile conical nozzles, a 22G sterile cylindrical nozzle, and a 20G sterile stainless steel cylindrical nozzle all with the same 30 mm length (see Table 3.1 for the technical specifications of the nozzles). The experiments performed with a material unit prepared using 1.2 mL of non-sterile TeloCol (6 mg/mL) as the

bioink, 0.5 mL of TeloCol neutralization solution, and 0.65 mL of DMEM with 10% FBS and 1% Pen-strep, following the pre-set mixing values (see Fig. 3.2). For each condition, the initial run was performed with the pre-selected parameters, which were subsequently adjusted to find the optimal settings for each conical or cylindrical nozzle. Each iteration involved dispensing one row of a 96-well plate with 5 µL per well. The dispensing process was visually assessed using the printer's camera, and droplet centralization was evaluated scanning the plate together with a 96-well plate centralization layout (see Fig. 3.3). This hand-made layout features 4 concentric circles centered within the well. The positioning of the droplet in relation to these circles indicates its centralization: the more circles the droplet contacts, the less centralized it is. This layout allows for easy visual assessment of the droplet's centralization.

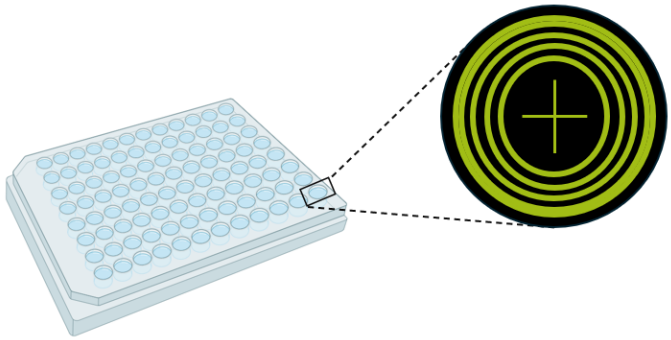

Figure 3.3: Visual representation of the 96-well plate layout to asses the droplet centralization displaying 4 concentric circles centered within the well.

Table 3.1: Optimization parameters.

Nozzle Type (color)	**Gauge**	**Outlet inner diameter (mm)**	**Material**
Conical nozzle (blue)	22	0.41	Polypropylene
Conical nozzle (pink)	20	0.58	Polypropylene
Conical nozzle (green)	18	0.84	Polypropylene
Cylindrical nozzle (blue)	22	0.41	Polypropylene and stainless steel
Cylindrical nozzle (uncolored)	20	0.58	Stainless steel

3.4 Cell studies

To assess the performance of BIO CELLX to examine if it can be a candidate to be high-throughput bioprinter, it is essential to conduct cell studies focusing on cell viability and the distribution of cell density across prints. Throughout all experiments,

mesenchymal stem cells (MSCs) tagged with a constitutively red fluorescent protein, mCherry, were used, specifically the ASC52 cell line. This cell line, obtained from the American Type Culture Collection (ATCC), is a human telomerase reverse transcriptase (hTERT) immortalized adipose-derived MSC line that exhibits a fibroblast-like morphology. The cells were originally isolated from the adipose tissue of a white female in 2006.

3.4.1 Cell culture

The cell line was thawed by warming the vial with the hands until only a small piece of ice remained. The solution was then resuspended, and the entire content was transferred to a Falcon tube. It was mixed with DMEM containing 10% FBS and 1% Pen-Strep, and centrifuged at 1000 rpm for 4 minutes. The supernatant was discarded, and the pellet was resuspended in fresh cell media. The entire content was transferred to a flask and incubated at 37°C and 5% CO_2.

The flask was inspected using an Echo Revolve microscope, and the cell media was changed every three days. When cells reached sub-confluence (around 80%), the cells were trypsinized and re-seeded into new culture flasks with a proportion of 6.000 cells/m^2. For the trypsinization process, the cell media was removed, and phosphate-buffered saline (PBS) was added to the flask for a few seconds. After removing the PBS, trypsin was added and incubated for 5 minutes to ensure detachment of the MSCs from the flask. The flask was then gently tapped, and cell media was added to neutralize the trypsin. The entire content was transferred to a Falcon tube and centrifuged at 1000 rpm for 4 minutes. The supernatant was removed, and the pellet was resuspended in fresh cell media. To determine cell concentration, the Countess II Automated Cell Counter was used. Equal parts of Trypan Blue and cell suspension were mixed, and 10 µL of the mixture was added to one of the chambers in the Countess II Automated Cell Counter slide. The cell count was directly obtained, and the slide was moved to inspect different regions for an average concentration.

Once cell growth was observed to be stable and sufficient, the doubling time (T_d) of the cell line was calculated. This allowed for the determination of whether the current cell culture exhibited the same proliferation rate as indicated by ATCC for this specific line, thereby excluding any potential environmental alterations such as bacterial contamination. This was conducted following Equation 3.1, in which doubling time can be computed.

$$T_d = \frac{t \ln(2)}{\ln\left(\frac{N_t}{N_0}\right)} \tag{3.1}$$

where t is the incubation period, N_t is the number of cells at the end of the incubation time, and N_0 is the initial number of cells at the beginning of the incubation time. After verifying the doubling time, the cultures were ready to proceed with the cell culture studies.

3.4.2 Material unit preparation and dispensing

Upon reaching sub-confluency, the flask was trypsinized, and the cell concentration was calculated as previously described. At this point, a sterile material unit was prepared inside the LAF bench by using the pre-filled capsules of 1.2 mL of sterile TeloCol (6 mg/mL) as the bioink, and the 0.5 mL of TeloCol neutralization solution capsule, and adding 0.65 mL of cell suspension at a concentration of 0.5 million cells/mL. The pre-set parameters (see Fig. 3.2), along with specific adjustments, were applied to evaluate their effects (see Table 3.2). Two 96-well plates were printed for each condition: one with 24 droplets of 5 µL per well, and the second one with 80 µL per well until the material was exhausted. Once the crosslinking time was completed, the well-plate was removed and placed inside the LAF bench, where 150 µL of cell media was added to each well. The well-plate was then incubated.

Identical to the printed ones, well-plates were created using the hand-mixing procedure and manually casting the droplets as controls. In all experiments, 6 mg/mL of TeloCol were used. For each 1 mL of 6 mg/mL neutralized TeloCol, 600 µL of TeloCol I (10 mg/mL) and 200 µl of neutralization buffer were mixed for 20 pumps back and forward. After mixing the 6 mg/ml neutralized TeloCol was loaded into a 3 mL syringe, capped, and put on ice prior to cellular mixing. All the solutions, and materials for the collagen mixing was kept on ice during all steps. 700 µL mL of neutralized TeloCol (Advanced Biomatrix) was split in 2 syringes (3 mL, BD) containing 350 µL. using a female/female Luer lock adapter. 300 µL of cellular solution was loaded into 1 of the syringes. After connecting both syringes with the Luer lock, 20 pumps 20 pumps back and forward were performed manually. Cell/ neutralized TeloCol mix was ready to be casted by positive displacement pipetting.

3.4.3 Cell viability staining

This assay was performed to evaluate the viability of the MSCs after printing, specifically at 1, 4, and 7 days post-printing. This allowed for the detection of any immediate or delayed cell damage resulting from the printing process. For each staining day, 4 droplets per condition were selected for staining from the well plate containing 5 µL droplets, with an additional well from the hand-mixed plate serving as a negative control. For the negative control, the cell media was removed, and 150 µL of 70% isopropyl alcohol (IPA) was added, followed by a 10-minute incubation. After this step, the cell medium and the IPA was removed from the wells selected for staining, and the wells were washed twice with 150 µL of Hanks' Balanced Salt Solution (HBSS) (+/+). The HBSS (+/+) was then removed, and the samples were stained with Hoechst at a concentration of 0.3 µg/mL in HBSS (+/+) solution, along with 2 drops of NucGreen per mL, and incubated for 5 minutes. After staining, the solution was removed, and 150 µL of HBSS (+/+) was added to each well and incubated for another 10 minutes. Finally, the samples were washed with HBSS (+/+) one last time.

After staining, the samples were imaged using an Echo Revolve microscope. The bright field was used to center the well at 4x magnification. Fluorescence channels

Table 3.2: Description of the conditions and modified variables for each of the four experiments.

Experiment number	Conditions	Modified variables
1	Control	Hand mixing and dispensing
	4 mix	None
	8 mix	8 cell mixing cycles
2	Control	Hand mixing and dispensing
	4 mix	None
	8 mix	8 cell mixing cycles
3	Control	Hand mixing and dispensing
	4 mix	None
	8 mix	8 cell mixing cycles
4	Cylindrical nozzle	20G stainless steel cylindrical nozzle, 15 µL/s extrusion and retraction rate, 15 µL retraction volume, and 0.6 mm z-offset.
	Cylindrical nozzle 4 hours after mixing	20G stainless steel cylindrical nozzle, 15 µL/s extrusion and retraction rate, 15 µL retraction volume, 0.6 mm z-offset, and dispensed 4 hours after mixing.

were selected: Texas Red (TXRED) was used for MSCs tagged with a red fluorescent protein, Fluorescein Isothiocyanate (FITC) for cells stained with NucGreen, and 4',6-diamidino-2-phenylindole (DAPI) for Hoechst dye. A representative section along the vertical axis was identified for each sample, with images taken every 60 µm from all channels. These images were then overlaid to create a Tag Image File Format (TIFF), which was saved and later analyzed with ImageJ. This software enabled the counting of live cells (red), dead cells (green), and total cells (blue), allowing for the calculation of final viability for each sample.

3.4.4 Cell homogeneity assay

The evaluation of the mixing homogeneity and dispensing accuracy can be conducted using a metabolic assay. For this task, the cell viability reagent Presto Blue can be used to measure the metabolic activity of cells. Live cells are able to reduce a compound called resazurin in a fluorescent product called resorufin, but this can only been done by viable cells. Thus, a well with a higher concentration of cells will

produce more fluorescence activity than one with fewer cells.

To perform this experiment, the 96-well plate with 80 µL samples was utilized. First, the cell media was removed from all wells and replaced with 150 µL of cell media containing 10% Presto Blue. The well-plate was then incubated, and fluorescence activity was measured after 3, 5, and 6 hours using a fluorescence reader to control and detect the most accurate time in which the fluorescence activity is more reliable. The data was later extracted for post-processing.

4

Results

The results for validation, optimization, and cells studies are presented in this section, following the same structure as explained in the methodology.

4.1 Validation

The screening process performed for evaluating the workflow performance of BIO CELLX, together with the outcome obtained from its droplet accuracy, evaporation assessment, and pH evaluation are shown in this segment.

4.1.1 Workflow performance

The BIO CELLX workflow was evaluated and reported to other departments 46 times. From these evaluations, 78 errors related to software, hardware, and scientific applications were encountered (see Table 4.1). As can be observed in Figure 4.1, the five most common errors represented the 65% of the total issues found. The most frequent error was the absence of extrusion, occurring 18 times, followed by an ABL failure with 12 times. All errors were reported to the relevant department, and another iteration was performed once feedback was received.

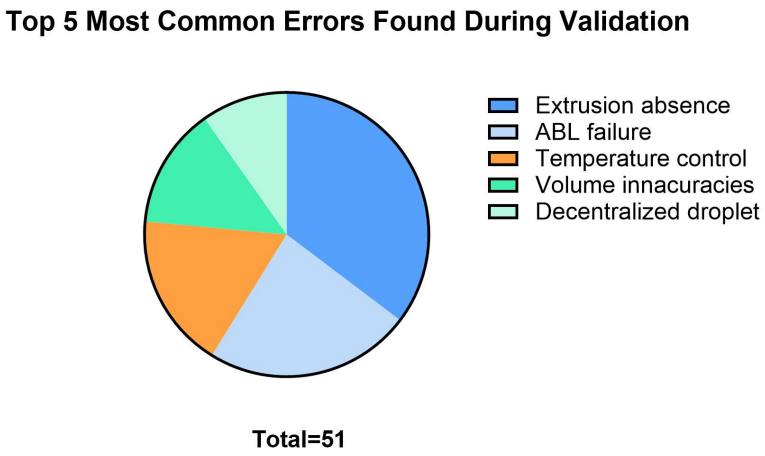

Figure 4.1: The five most prevalent issues encountered during validation were absence of extrusion in dark blue (18 times), ABL failure in clear blue (12 times), temperature control in orange (9 times), volume inaccuracies in dark turquoise (7 times), and decentralized droplet in clear turquoise (5 times).

Table 4.1: Errors found during BIO CELLX validation, categorized by departments and occurrence count.

Area	Errors encountered	Number of times
Software	Absence of extrusion, temperature control, camera malfunction, connectivity errors, User Interface crash, fans miss regulation, printbed collision, and leakage during channel priming	41
Hardware	ABL failure, piston faulty maneuver, cartridge station opening failure, nozzle cap incorrect deposition, and snap plunger incorrect attachment	20
Scientific Applications	Decentralized droplet, residue on the nozzle, and volume inaccuracies	17

4.1.2 Droplet accuracy

From the tests performed in BIO CELLX using Mili-Q water, the dispensing for 5 µL droplets showed an average of 4.73 µL, a standard deviation (SD) of 0.13 µL, a CV of 2.66%, and an accuracy of 94.7%. For the 2.5 µL, the average was 2.39 µL, the SD was 0.13 µL, the CV was 5.33%, and an accuracy was 95.54%. Lastly, the 1 µL droplets presented an average of 0.92 µL, a SD of 0.05 µL, a CV of 5.66%, and an accuracy of 92.28% (see Figure 4.2).

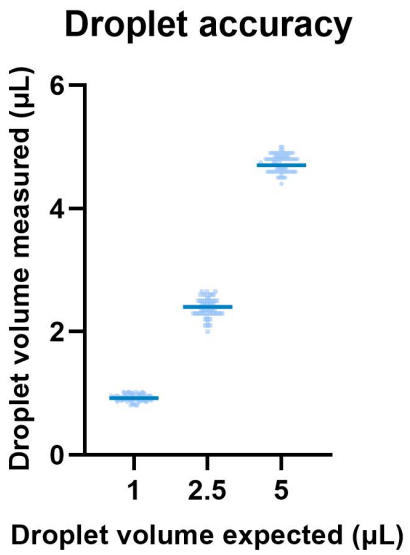

Figure 4.2: Volume measured for 96 Milli-Q water droplets each of 1 µL, 2.5 µL, and 5 µL (clear blue), with the corresponding median values indicated (dark blue).

4.1.3 Evaporation assessment

The droplet evaporation during the workflow for a 384-well plate using non-sterile alginate (6 mg/mL) was evaluated for 1 µL and 5 µL volumes. For the 1 µL droplets, an average gain in volume of 0.7 µL was observed, with a SD of 13.89 µL and a CV of 1984.63%. For the 5 µL droplets, an average reduction in volume of 4.89 µL was observed, with a SD of 21.22 µL and a CV of 434.19% (see Figure 4.3).

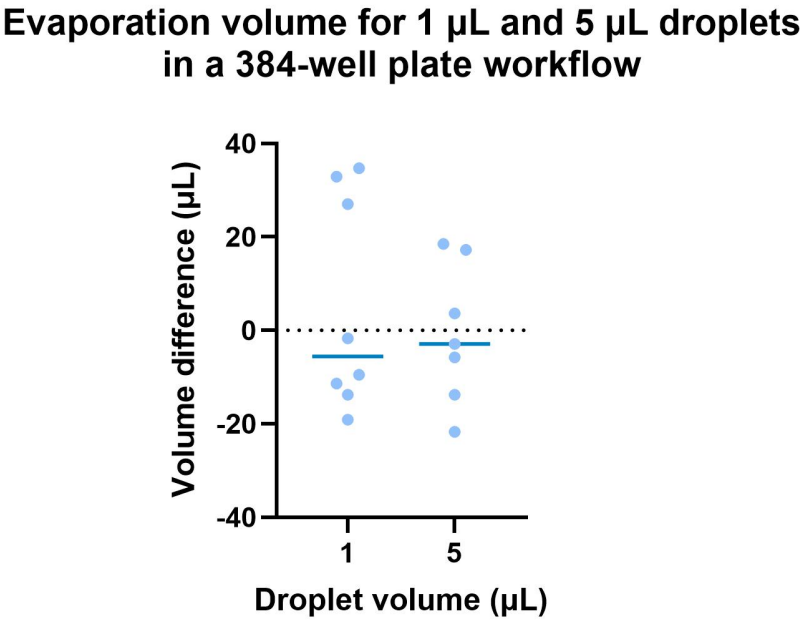

Figure 4.3: Volume difference before and after a 384-well plate workflow with alginate (6 mg/mL) droplets of 1 µL and 5 µL (clear blue), with the corresponding median values indicated (dark blue).

4.1.4 pH evaluation

For the evaluation of the pH values after 20 bioink mixing cycles and 4 cell mixing cycles, two colorimetric tests were used: pH Duotest and pH Fisherbrand test. From visual inspection, it was determined that the nine samples of TeloCol (6 mg/mL), each with 200 µL, showed a pH between 7.1 and 7.4 according to the Duotest and a pH of 7 according to the Fisherbrand test. Moreover, no difference was detected between the printed samples and the control (see Figure 4.4).

4.2 Optimization

To optimize the dispensing process with BIO CELLX, the dispensing parameters were adjusted and the outcomes were evaluated iteratively.

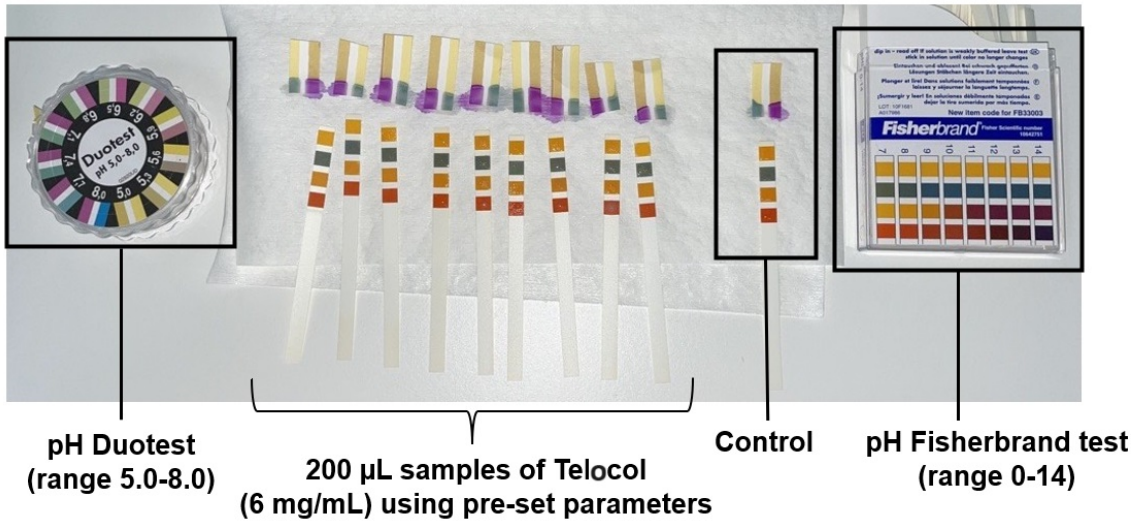

Figure 4.4: TeloCol (6 mg/mL) samples along with the hand-mix control evaluated by the pH Duotest with a detection range between 5.0 and 8.0, and the pH Fisherbrand test with a detection range between 0 and 14.

4.2.1 Dispensing parameters

Within the material configuration screen, the extrusion rate, retraction rate, and Z-offset were fine-tuned to achieve better droplet centralization and avoid common issues detected during dispensing (see Figure 4.5). A total of three conical nozzles and two cylindrical nozzles were tested, resulting in the optimal dispensing parameters shown in Table 4.2. The centralization of the droplets was assessed by scanning the well plate using a 96-well plate with a concentric circle layout. The average number of contact circles for each nozzle type was as follows: 22G conical nozzle contacted 3 circles, 20G conical nozzle contacted 1.5 circles, 18G conical nozzle contacted 1.88 circles, 22G cylindrical nozzle contacted 3.63 circles, and the stainless steel 20G cylindrical nozzle contacted 2.75 circles. In Figure 4.6 some of the best outcomes for each nozzle type are displayed. The 20G conical nozzle showed the best results, followed by the 18G conical nozzle and the 20G stainless steel cylindrical nozzle.

Table 4.2: Optimal dispensing parameters found for the conical nozzles 22G, 20G, and 18G, and for the cylindrical nozzle 22G and 20G.

Nozzle Type (gauge)	**Extrusion and retraction rate (µL/s)**	**Retract volume (µL)**	**Z-offset (mm)**
Conical nozzle (22G)	20 and 20	10	0.5
Conical nozzle (20G)	20 and 20	10	0.6
Conical nozzle (18G)	15 and 15	10	0.8
Cylindrical nozzle (22G)	15 and 15	15	0.5
Cylindrical nozzle (20G)	15 and 15	15	0.6

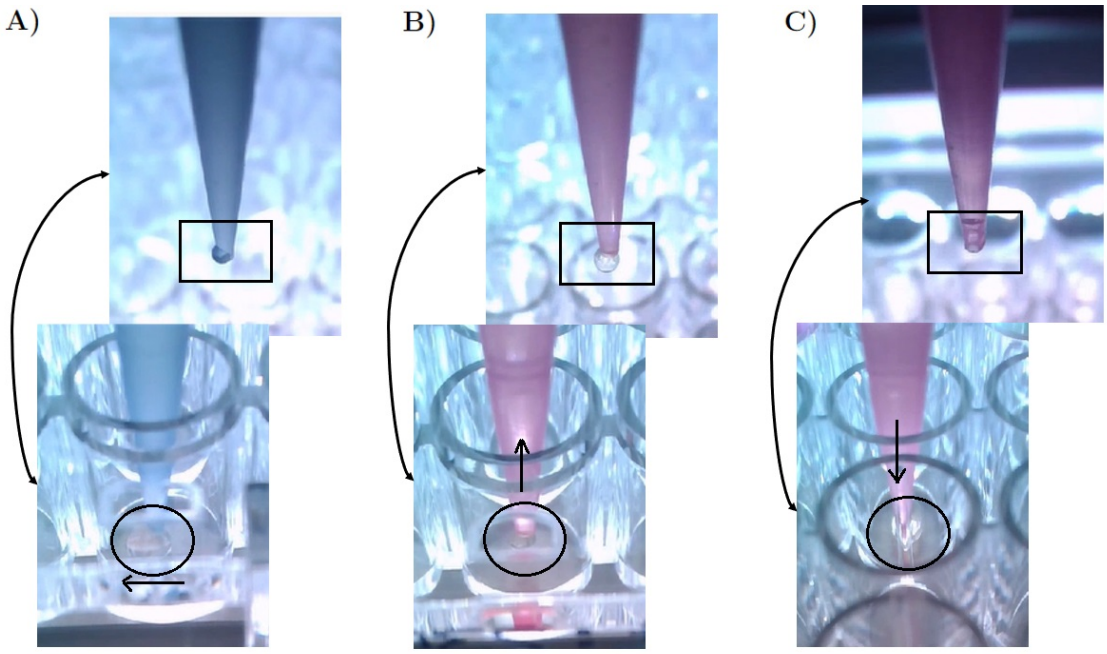

Figure 4.5: Recurrent problems that occur during dispensing and affect the results of the print. A) A droplet slips off the well plate surface, resulting in a droplet on the side and residue on one side of the nozzle (conical nozzle 22G with pre-set values). B) Dispensing too high on the Z-axis, which does not touch the well plate and carries the remaining drop to the next well (conical nozzle 20G with pre-set values but Z-offset at 0.7 mm). C) Dispensing too low, resulting in a lot of residue on the nozzle (conical nozzle 20G with pre-set values but Z-offset at 0.3 mm).

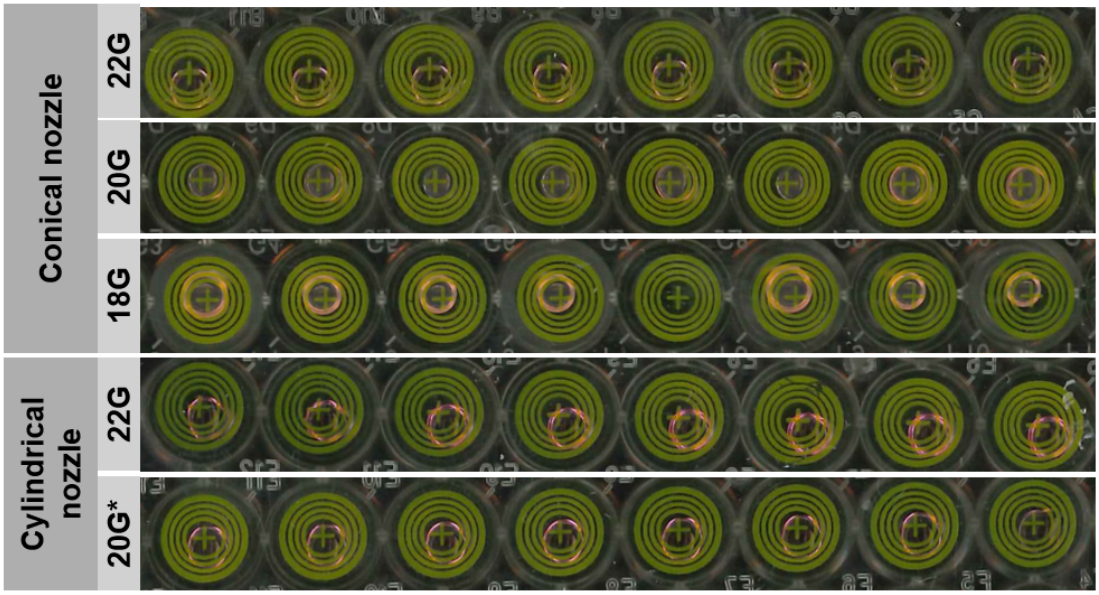

Figure 4.6: Representative picture of droplet centralization using different nozzle types.

4.3 Cell studies

The dispensing with cells and their behavior was studied using MSCs. The effects of increasing cell mixing cycles, using cylindrical nozzles, and dispensing after certain time intervals were examined.

4.3.1 Cell viability

To compute the viability of the different experiments performed, the number of live cells (red), dead cells (green), and total cells (blue) were counted in each case.

4.3.1.1 Cell mixing cycles (Experiment 1, 2, and 3)

The experiment conducted to compare cell behavior with an increased number of cell mixing cycles in TeloCol (6mg/mL) was performed three times. The viability results for each experiment can be seen in Figures A.2A, A.4A, and A.5A. They have the following viabilities: on Day 1, control showed a viability of 94.74% ± 1.34%, 4 cell mixing cycles condition showed a viability of 92.81% ± 0.63%, and the 8 cell mixing cycles condition showed a viability of 93.81% ± 1.55%. On Day 4, the control case presented a viability of 93.52% with a SD of 3.66%, the 4 cell mixing cycles condition showed a viability of 95.05% ± 1%, and the 8 cell mixing cycles condition showed a viability of 96.43% ± 0.27%. Finally, on Day 7, the control case showed a viability of 88.69% ± 1.68%, the 4 cell mixing cycles condition showed a viability of 90.85% ± 2.16%, and the 8 cell mixing cycles condition showed a viability of 92.31% ± 0.83%.After performing unpaired t-tests and ordinary one-way Analysis of Variance (ANOVA) tests between conditions, no statistically significant differences were found, with all P-values exceeding 0.05.

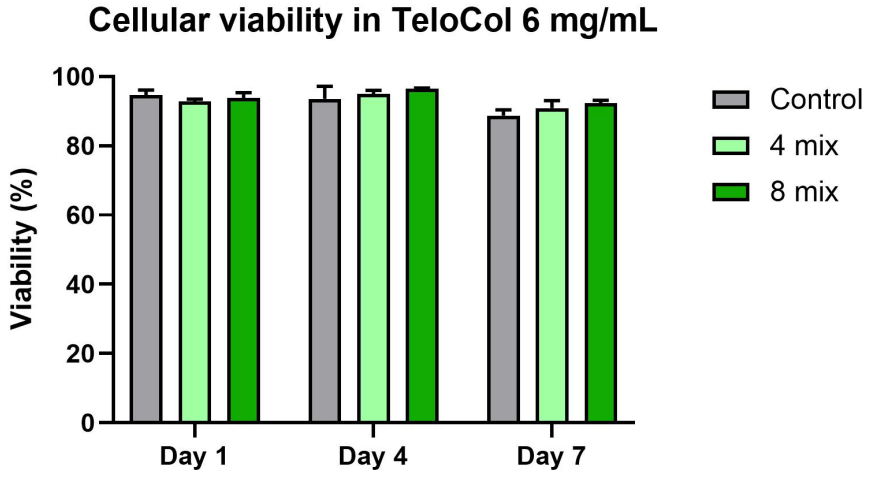

Figure 4.7: Viability percentage of cells embedded in TeloCol (6 mg/mL) droplets at day 1, 4 and 7 days after different mixing conditions (4 or 8 times) compared to control (hand-dispensed). Data is shown as average ± standard deviation.

Additionally, the ratio between live and dead cells for each condition, normalized to day 1, can be observed in Figure 4.8 (to visualize each experiment per separate see Fig. A.2B, Fig. A.4B, and Fig. A.5B.

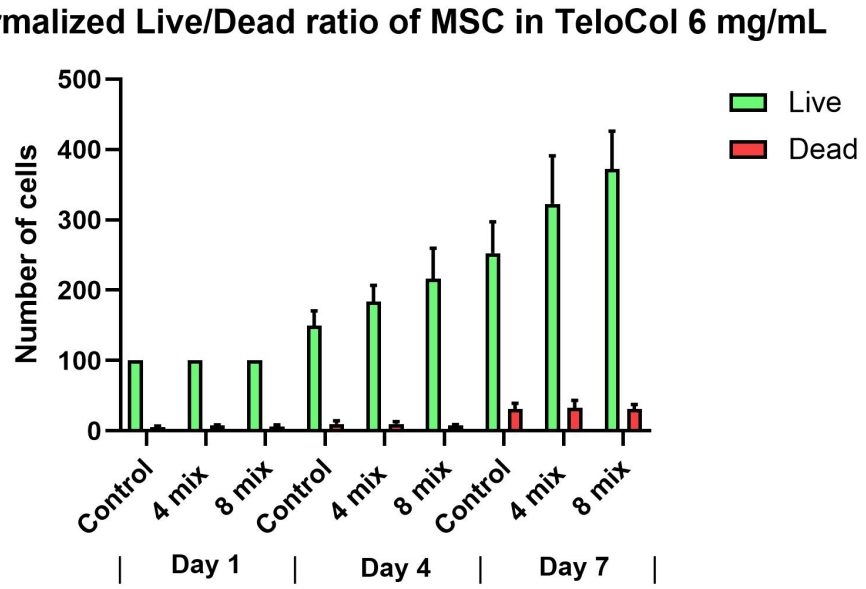

Figure 4.8: Ratio of live cells (green) and dead cells (red) of embedded in TeloCol (6 mg/mL) droplets at day 1, 4 and 7 days after different mixing conditions (4 or 8 times) compared to control (hand-dispensed)

Through the microscope, cells can be observed directly to appreciate the changes between days and conditions. For instance, in Figure 4.9, it is observed the changing ratio of live cells, dead cells, and total cells between days 1, 4, and 7. It also compares the control sample with those subjected to 4 and 8 cell mixing cycles (see Figures A.3 and A.6 for Experiments 1 and 3, respectively). Moreover, using bright field imaging, not only changes can be distinguished between droplets in the same condition but also at different incubation days. This is illustrated in Figure 4.10, which compares 5 µL TeloCol (6 mg/mL) droplets exposed to 4 cell mixing cycles on days 1 and 7. Additionally, changes can be detected in MSCs spreading in 2D compared to the same cells spreading in 3D (see Figure 4.11).

4.3.1.2 Cylindrical nozzle and sedimentation analysis (Experiment 4)

To analyze the effect of cylindrical nozzle in the cell behaviour, the same tests performed in the previous section were conducted but with only one repetition. Therefore, the viability for the 20G cylindrical nozzle using the pre-set parameters was 96.29% for day 1, 95.86% for day 4, and 91.53% for day 7 (see Fig. 4.12). Moreover, the live to dead ratio of cells per day normalized to day 1 can be seen in Figure 4.13 and the the evolution over the days through the microscope in Figure 4.14.

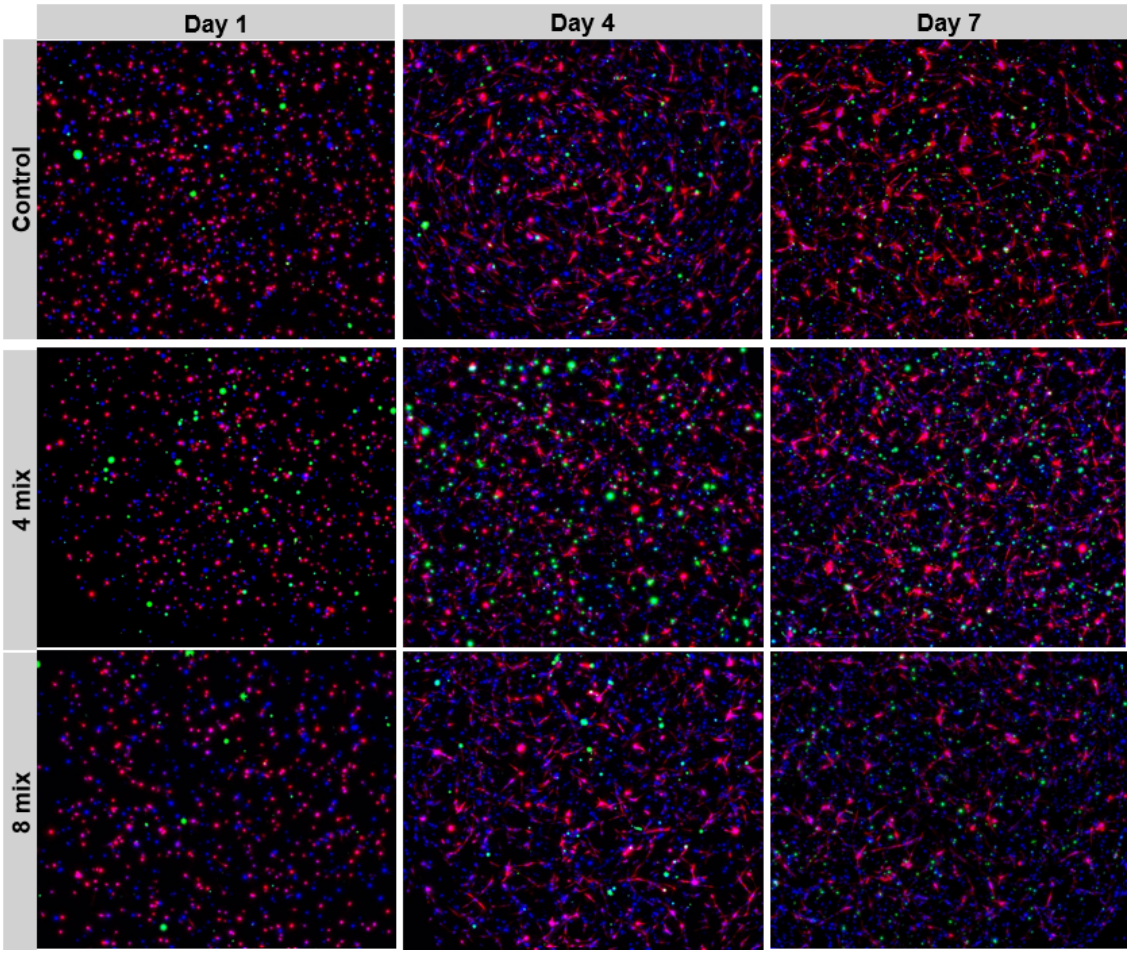

Figure 4.9: Cell viability (live in red, dead in green, nucleus in blue) of printed droplets in Experiment 2 of printed droplets after mixing TeloCol and cells using the BIO CELLX or standard syringe to syringe mixing protocol. Representative pictures were taken after 1, 4 and 7 days for the BIO CELLX printed droplets and for the standard mixing protocol respectively. Pictures were obtained using the ECHO Revolve microscope with FITC, TEXAS RED, and DAPI filters at 4X.

4.3.2 Cell homogeneity

The distribution of cell density during the printing was evaluated measuring the metabolic activity.

4.3.2.1 Cell mixing cycles (Experiment 1, 2, and 3)

As shown in Figure 4.15, the CV between the metabolic activity of the wells for 80 µL TeloCol (6 mg/mL) droplets in different mixing conditions was found to be 19.16% after 3 hours of incubation for the control case, 12.93% for the samples exposed to 4 cell mixing cycles, and 10.93% for the samples exposed to 8 cell mixing cycles. After 5 hours of incubation, the control presented a CV of 10.63%, the 4 mixing cycles presented 7.98%, and the 8 mixing cycles presented 8.42%. Lastly, after 6 hours, the control had a CV of 9.03%, the 4 mixing cycles had 6.62%, and

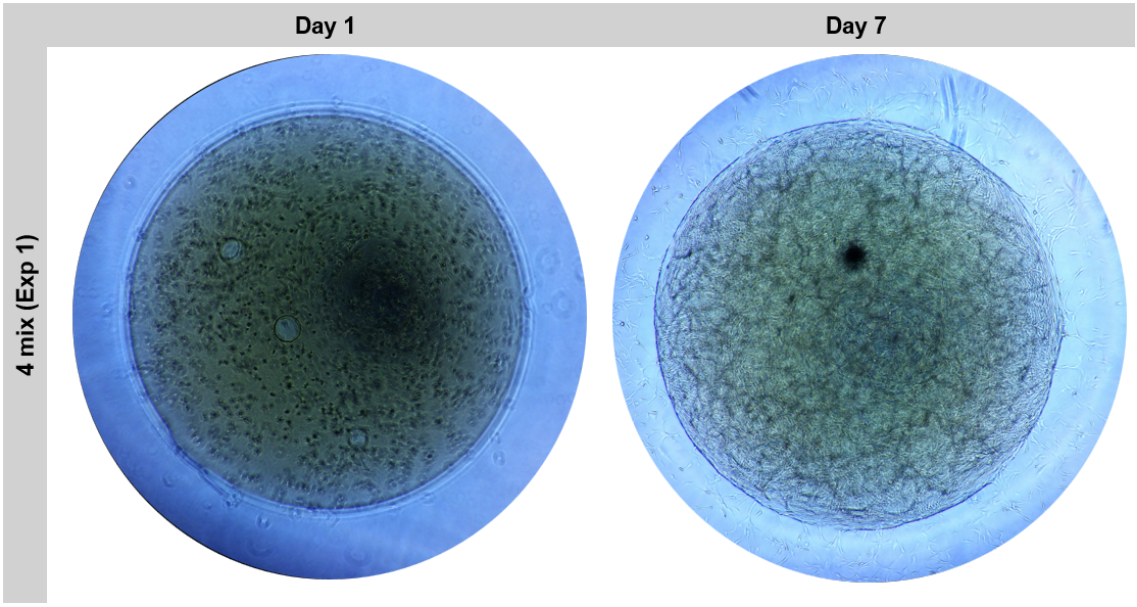

Figure 4.10: Comparison of 5 µL TeloCol (6 mg/mL) droplet printed after 4 cell mixing cycles in day 1 (left) and day 7 (right) both at 4x magnification.

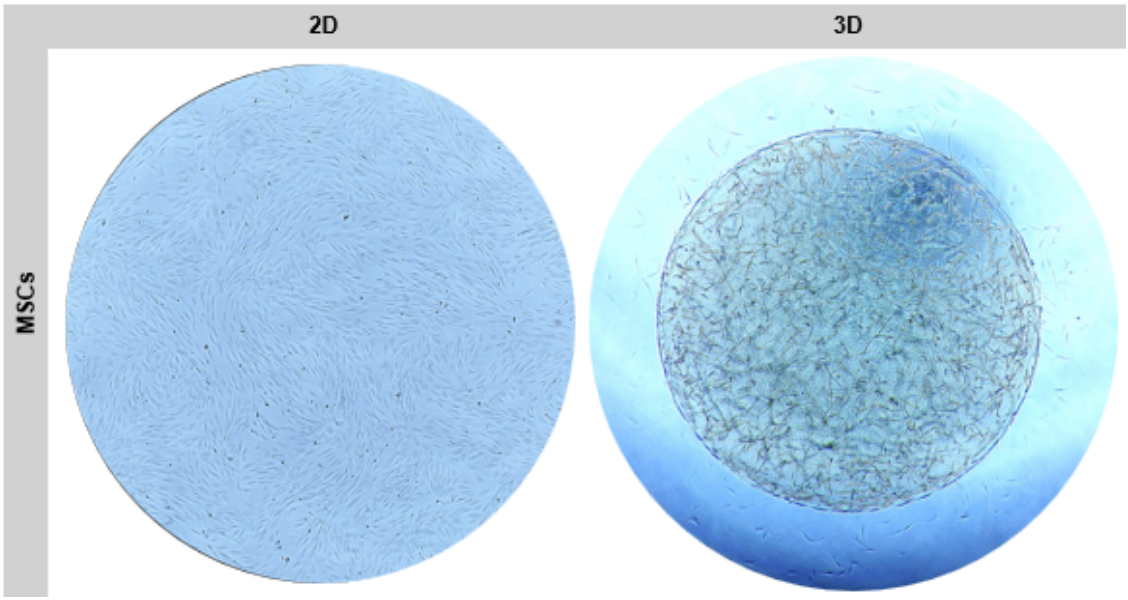

Figure 4.11: Comparison of MSCs proliferation between 2D expansion stage in a T-flask (left) and 3D in a 5 µL TeloCol (6 mg/mL) droplet exposed to 8 cell mixing cycles in day 17 of incubation (right) both at 4x magnification.

the 8 mixing cycles had 7.19%. Furthermore, for each condition and experiment, the fluorescence activity, SD, and the signal-noise-to ratio evolution can be observed along the incubation time. This can be seen in Figure 4.16 for the control condition in Experiment 3. To observe all the other conditions for Experiment 1, see Figures A.7, A.8, and A.9; for Experiment 2, see Figures A.10, A.11, and A.12; and for Experiment 3, see Figures A.13 and A.14.

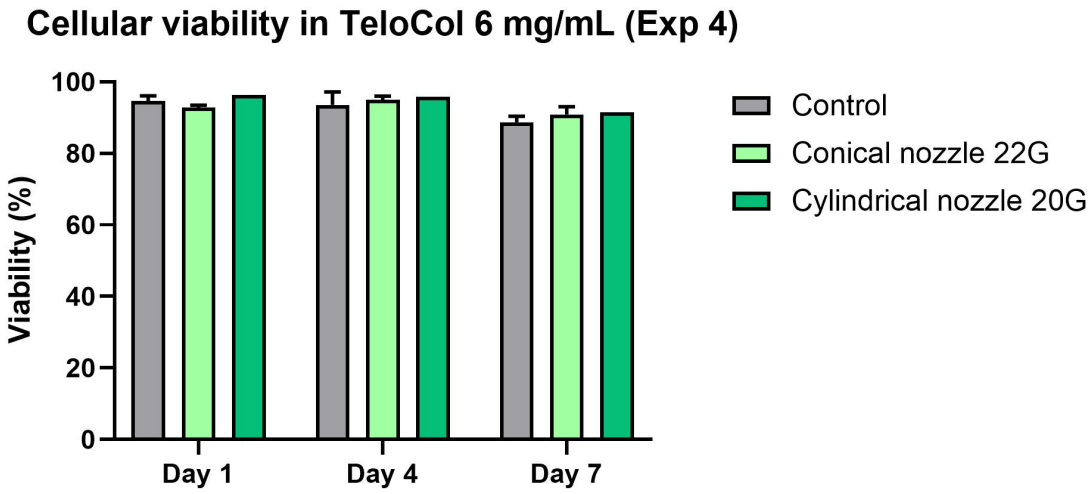

Figure 4.12: Viability percentage of cells embedded in TeloCol (6 mg/mL) droplets at day 1, 4 and 7 days after different nozzle conditions (conical or cylindrical) compared to control (hand-dispensed). Data is shown as average ± standard deviation.

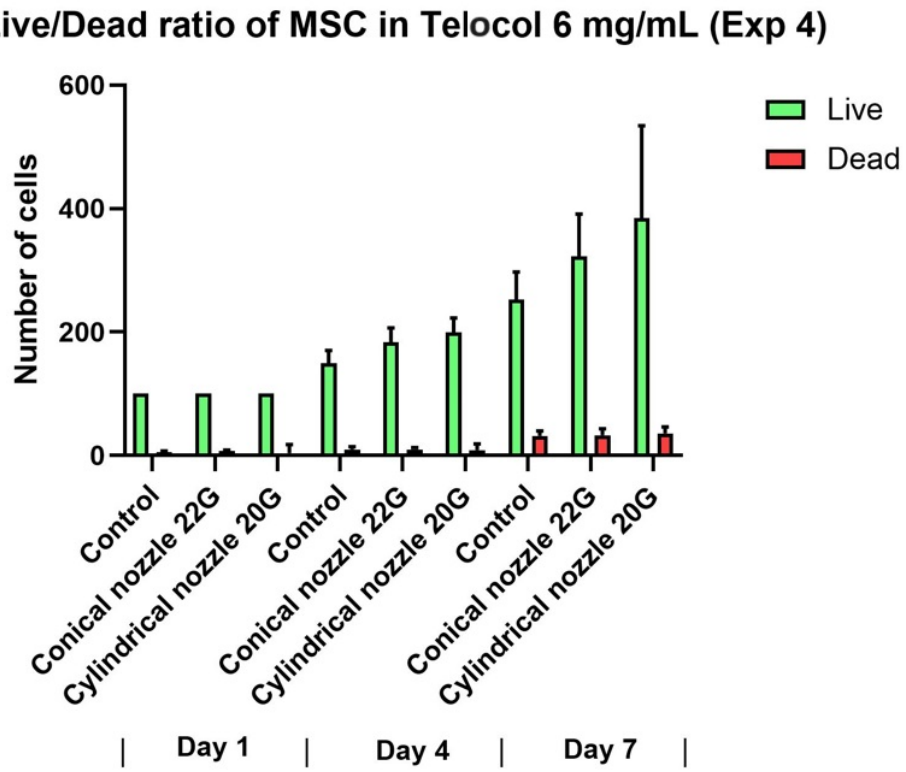

Figure 4.13: Ratio of live cells (green) and dead cells (red) of embedded in TeloCol (6 mg/mL) droplets at day 1, 4 and 7 days after different nozzle conditions (conical or cylindrical) compared to control (hand-dispensed).

4.3.2.2 Cylindrical nozzle and sedimentation analysis (Experiment 4)

Regarding the cylindrical nozzle, the investigation aimed to explore the difference in cell density between wells when printing occurs 4 hours after mixing to detect if

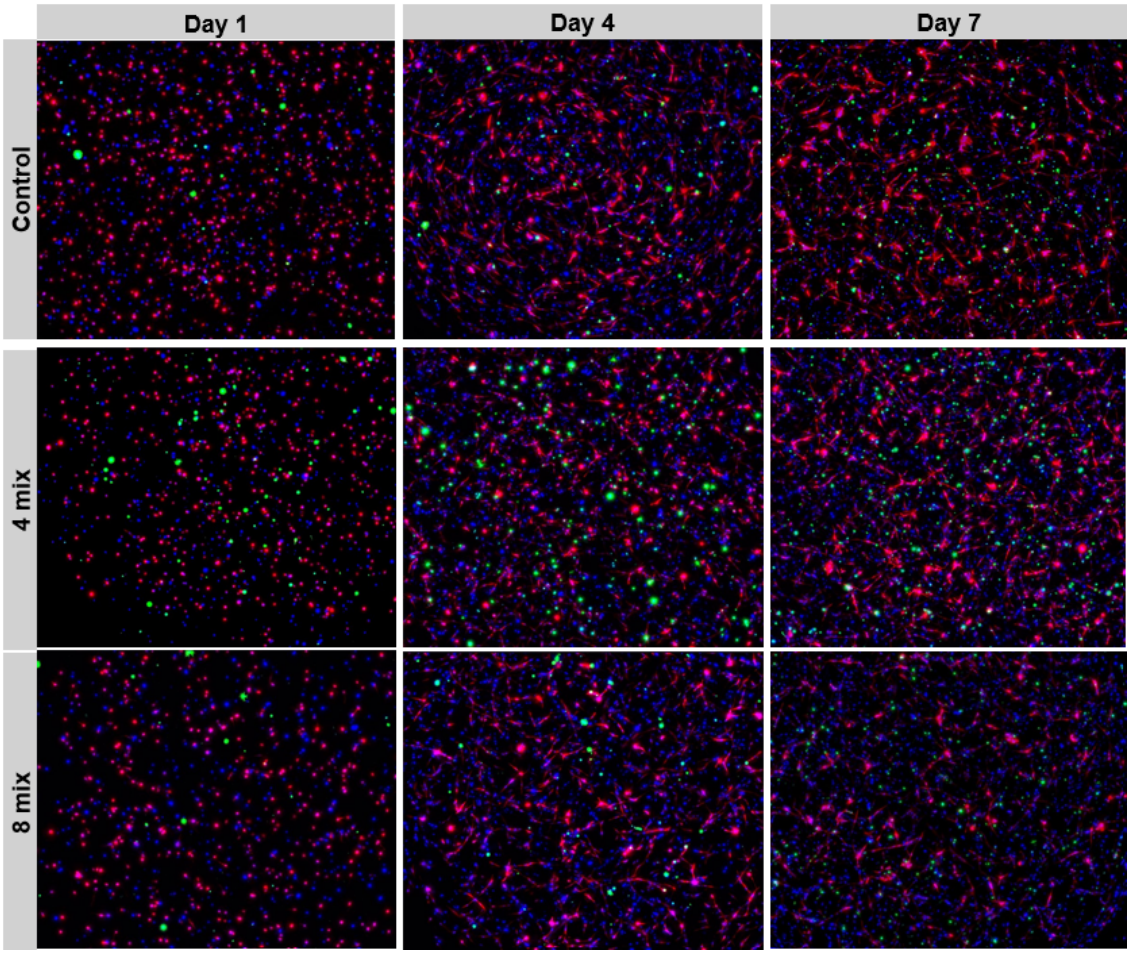

Figure 4.14: Cell viability (live in red, dead in green, nucleus in blue) of printed droplets in Experiment 4 after mixing TeloCol and cells using the BIO CELLX or standard syringe to syringe mixing protocol. Representative pictures were taken after 1, 4 and 7 days for the BIO CELLX printed droplets and for the standard mixing protocol respectively. Pictures were obtained using the ECHO Revolve microscope with FITC and DAPI filters at 4X.

the cells sediment in telocollagen. As presented in Figure 4.17, the CV when samples are dispensed 4 hours after mixing differs from the values obtained previously with the conical nozzle under the same mixing conditions, but printed immediately after mixing (4 mix condition of Experiments 1, 2, and 3). In this case, the CV was 19.94% after 3 hours of incubation, 17.77% after 5 hours, and 16.61% after 6 hours. Additionally, the fluorescence activity across the wells following the printing sequence can be compared between conditions, as shown in Figure 4.18.

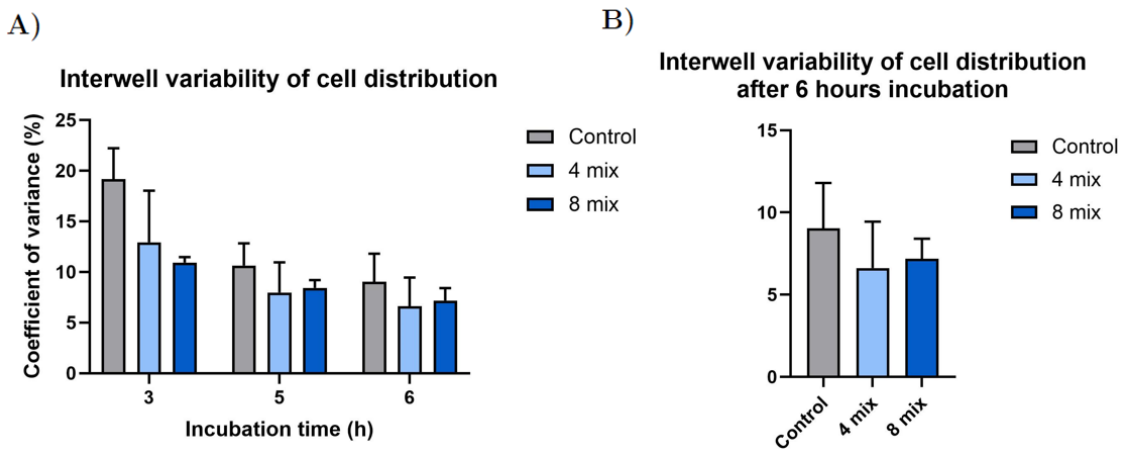

Figure 4.15: Coefficient of variance (%) of fluorescence signal from cells distributed across wells comparing different mixing conditions. The error bars representing the standard deviation between the three repetitions of the experiment. Cells embedded in 80 µL TeloCol (6 mg/mL) were incubated with Prestoblue for A) Across three incubation times: 3, 5, and 6 hours. B) For 6 hours of incubation.

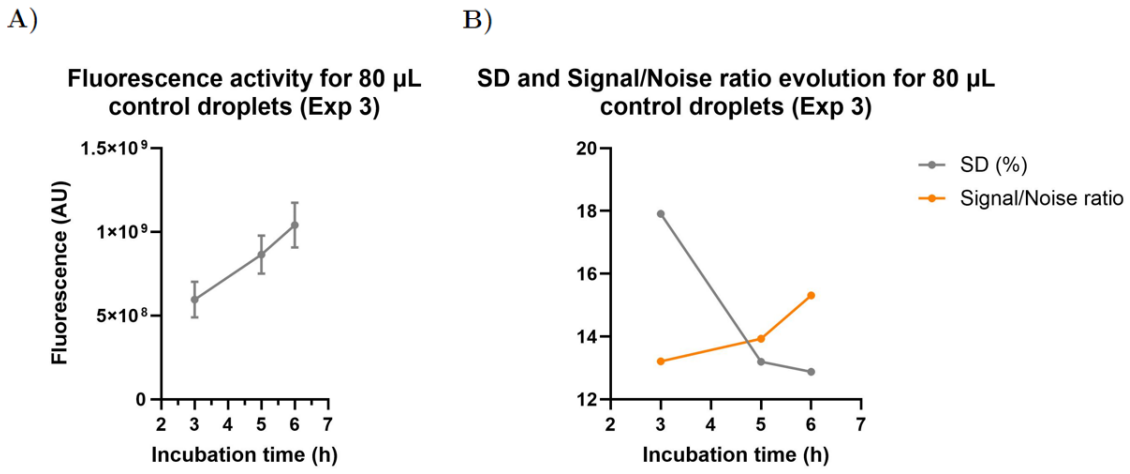

Figure 4.16: Control parameters from homogeneity Experiment 3 in the control condition. A) Evolution of fluorescence activity expressed as relative fluorescence activity in arbitrary units (AU) over incubation time. B) Evolution of the standard deviation (SD) and the signal to noise ration over incubation time.

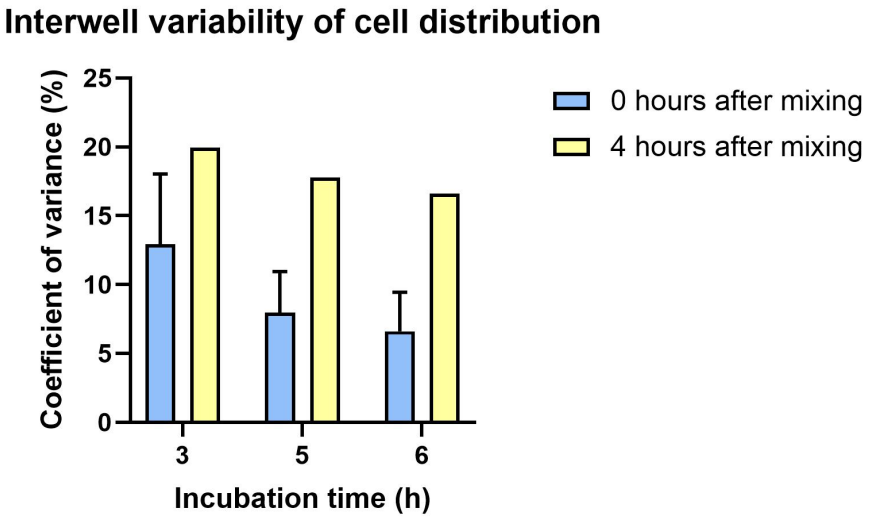

Figure 4.17: Coefficient of variance (%) of fluorescence signal from cells distributed across wells comparing different mixing conditions. The error bars representing the standard deviation between the three repetitions of the experiment. Cells embedded in 80 µL TeloCol (6 mg/mL) were incubated with Prestoblue across three incubation times: 3, 5, and 6 hours. In blue the droplets were exposed to 4 cell mixing cycles and dispensed immediately after mixing with a conical nozzle, and in yellow exposed to 4 cells mixing cycles and dispensed 4 hours after mixing with a cylindrical nozzle.

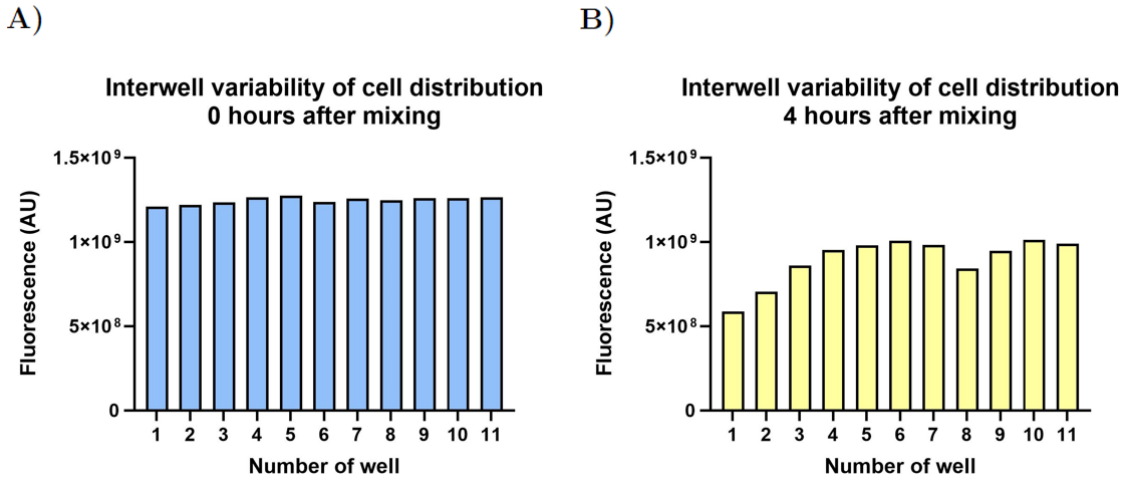

Figure 4.18: Fluorescence activity expressed as relative fluorescence activity in arbitrary units (AU) across the wells following the printing sequence. Cells embedded in 80 µL TeloCol (6 mg/mL) were incubated with Prestoblue for 6 hours. In blue the droplets were exposed to 4 cell mixing cycles and dispensed immediately after mixing with a conical nozzle, and in yellow exposed to 4 cells mixing cycles and dispensed 4 hours after mixing with a cylindrical nozzle.

5
Discussion

The main objective of this study was to evaluate the essential elements necessary for implementing BIO CELLX as a high-throughput bioprinter and to explore possible optimizations for improving its performance. To achieve this, four research questions were formulated at the start, with the aim of finding possible answers throughout the duration of the study. The first research question focused on validating the printer's workflow and identifying any potential issues related to software or hardware. The second question examined how dispensing parameters could be adjusted to prevent the droplet contact with the well walls and minimize evaporation. The third and fourth questions aimed to understand how cell behavior might change with alterations to the printing procedure, specifically the number of cell mixing cycles and the use of different nozzle types. In this section, these research questions are discussed to elucidate possible answers and challenges encountered during the study.

5.1 Functional and reliable workflow

It is reasonable to consider that when a customer acquires a new product, it is expecting a functional item that meet the expectations created. However, when new technologies emerge, reliability can become an issue since the procedures are not yet well established and experience in the field is understandably limited. BIO CELLX is no exception. Considering this, the need for a validation stage becomes evident to ensure that all the steps in the procedure are conducted as planned during the development and that the outcome meets the expectations.

In this study, the BIO CELLX workflow was tested 46 times, with most attempts revealing multiple issues. To improve the system, each run was documented and sent to the relevant departments for feedback, together with meetings to discuss the current state and future steps. Throughout the study, three different software versions were tested as continuous improvements were made to bring BIO CELLX closer to a reliable stage. Although some errors were random and isolated, the majority were recurrent. Of the 78 errors encountered, 51 were related to just five persistent issues (see Fig. 4.1). Within this 65% of cases, issues such as extrusion absence, often due to motor problems, and temperature control challenges, linked to software implementation, were eventually resolved in the latest version. Nevertheless, some issues, such as ABL failure, were found to be more complex and require the integration of a second recalibration of the printbed axis after the well plate is attached,

due to unintentional user movements. In cases of dispensing issues, such as volume inaccuracies or droplet decentralization, process optimizations are needed, but these issues are often multifactorial and difficult to completely resolve.

It is important to consider that BIO CELLX workflow is highly complex, involving precise mechanical components that handle micro-volume measurements and extremely controlled software that executes all necessary actions while keeping the user informed throughout the process. Accordingly, a close work between departments it is essential, requiring a basic understanding of all the parts involved to fully comprehend each step of the process. Additionally, implementing changes can be challenging, as they may involve existing hardware limitations or the development of new software features, often leading to long development periods. Nevertheless, after the validation and problem-solving efforts conducted from all the departments during this study, the final optimized version is fully functional, and complete workflows can be executed as demonstrated in the cell studies section. However, to ensure continued reliability, ongoing implementations and validations are necessary.

5.2 Features evaluation and optimization

Meeting all the demanding requirements to print in a 384-well plate is not an easy task, especially when dealing with a highly automated bioprinter. Accordingly, it was key to perform screenings to evaluate the current features of BIO CELLX and to adjust parameters for even better performance. To assess the quality of the mix and the dispensing, a pH evaluation and droplet accuracy tests were conducted.

During all the validation process, the mixing was observed to be well executed, with no bubbles or unmixed parts detected. However, it was necessary to determine if the mix quality was sufficient to ensure cell survival. Therefore, the pH evaluation was conducted and the results confirmed that the mix did not constitute a problem, as the pH was found to be between 7.1 and 7.4 (see Fig. 4.4), and accordingly to literature the most suitable range established for mammalian cells proliferation is moderately alkaline in between 7.0 and 7.2 [40]. To assess the precision of the dispensing, the droplet volume accuracy for 5, 2.5, and 1 µL was tested, resulting in CV of 2.66%, 5.33%, and 5.66%, respectively (see Fig. 4.2). As expected, the CV increases as the droplet volume decreases, since controlling smaller volumes is more challenging and errors have a greater impact. Nevertheless, all obtained values, including the 1 µL droplets, meet the technical requirement specifications (TRS) set for BIO CELLX, which states that for volumes between 5 to 1 µL, the CV must be lower that 7% and should be lower than 5%. The TRS was established according to the guidelines for HTS Assay Validation published in the Assay Guidance Manual [25], which stipulates that the CV should not exceed 20% considering the entire workflow. Although the recommended limit may seem quite high, it must be considered that this value also includes possible inaccuracies from the user, such as pipetting errors, drug dilutions, or cell concentration calculations as well as any potential variations that may occur within the bioprinter, such as evaporation.

So far, it is known that the droplets dispensed have an accurate volume and are properly mixed. However, considering that the dispensing and crosslinking steps for a 384-well plate can together take around 50 minutes, it is not unreasonable to assume that evaporation could occur. To evaluate this, an experiment was conducted to assess the volume lost after 50 minutes when the well-plate is inside the printer. As shown in Figure 4.3, the results were highly inconsistent, with some samples showing a decrease in weight and others even showing an increase. This gain in weight could be due to particle accumulation when the well-plate was transported from the bioprinter to the LAF hood for weighing, or due to condensation. The first hypothesis is less likely since a sterilization run was conducted before starting the experiment, the well-plate was transported using gloves, and the scale was inside the LAF hood, making particle accumulation particularly improbable. However, the second hypothesis is plausible. In hydrogels, such as TeloCol, water constitutes 90% of the total volume [41]. Additionally, the fact that the vessel and material are at 15°C during printing, combined with the unregulated temperature of the clean air in the chamber, could explain the observed weight gain. This highlights the problem of working with small volumes without a controlled enclosure space. Although BIO CELLX features a fully enclosed clean chamber with an HEPA filter, the temperature and humidity are not controlled. This can lead to evaporation or condensation of the droplets, resulting in several issues such as stability and integrity problems, volume inaccuracies, concentration changes, and potentially decreased cell viability due to increased macromolecule concentration, which could promote macromolecule crowding [42]. Consequently, more tests are needed to evaluate evaporation and condensation inside BIO CELLX, and it may also be necessary to implement a control system for temperature and humidity. Or as an alternative, reduce the printing time to avoid the possibility of evaporation and condensation, and improving the efficiency.

After the evaluation, the focus shifted to optimizing the dispensing process. To achieve this, three different conical nozzles and two cylindrical nozzles were tested, and their dispensing parameters were adjusted (see Table 4.2). The primary reason for this optimization was that the recommended nozzle, a 22G conical nozzle, showed significant challenges in producing a centralized droplet during validation. This issue was primarily due to the droplet slipping to one side of the nozzle (see Fig. 4.5A), causing the droplet to be off-center and leaving residue on one side of the nozzle, which affected the dispensing and centralization of the following wells. A possible explanation for this problem can be the effect of surface tension on droplet formation, particularly at the nozzle outlet. Since the 22G nozzle has a small opening, more surface area of the liquid is exposed to the air, resulting in higher surface tension and less bioink spreading. Consequently, the liquid tends to reduce this area by exhibiting stronger cohesive forces, forming more spherical droplets that can remain as residue on the nozzle [43, 44]. When the other nozzles, all with larger gauges, were tested, the results improved, possibly due to the lower surface tension and consequently to the different droplet shape. As shown in Figure 4.6, the 20G conical nozzle achieved the best centralization, followed by the 18G conical nozzle and the 20G stainless steel cylindrical needle. However, the parameters

were adjusted because the larger gauge required an increase in the z-offset to minimize contact between the liquid and the nozzle during dispensing, thereby reducing residue formation (see Fig. 4.5C). In the case of the cylindrical needle, dispensing is more challenging due to its straight pattern, which requires a lower extrusion and retraction rate, along with a higher retraction volume, to maintain greater control over the dispensing process and prevent leakages.

5.3 Cell behaviour under various conditions

To conclude the workflow, the process was conducted using MSCs, and the cell viability and distribution of cell density between prints were studied. Two different numbers of cell mixing cycles were investigated to determine if increased mixing cycles would result in reduced cell survival. The results were highly positive, with all conditions showing viability values close to or above 90% for days 1, 4, and 7 (see Figure 4.7), indicating no cytotoxic effect as all values exceeded 80% [45]. Furthermore, since the viability results showed no statistically significant differences between the control samples and those mixed with BIO CELLX, this can also indicate that additional cell mixing cycles did not negatively impact cell viability. The live/dead cell ratios, presented in Figure 4.8, showed a consistent increase in cell count over the 7-day cultivation period, with higher proliferation rates observed in samples exposed to 8 mixing cycles. When analyzing the three experiments separately, variations in cell numbers were observed, despite all showing a steady increase over the days. This discrepancy could be due to errors in cell counting or pipetting concentrations. Fluorescence microscopy images in Figures 4.9, 4.10, and 4.11 show cell stretching in the 4 and 8 mixing cycles, similar to the control group. Initially, some cells retained a rounded shape, but by day 4, all cells exhibited a healthy, stretched morphology. Additionally, the morphology of cells in 3D droplets differed from 2D cultures, with 2D cells appearing flat and elongated in a monolayer, while 3D cells maintained a natural shape with several layers. The stretched morphology of MSCs indicates proper cytoskeletal organization and cellular interactions, which are vital for cell signaling, differentiation, proliferation, and overall cell functionality [46]. This suggests that the pressure applied during the bioprinting process does not adversely affect the cells' morphology.

Regarding dispensing homogeneity, the best results were obtained six hours after incubation for all experiments, with low SD and high signal-to-noise ratio. The CV for the 4 and 8 mixing cycles was lower compared to the control in all three experiments, with values of 6.62% and 7.19% respectively, compared to 9.03% for the control. Although the CV for the 4 mixing cycles was slightly lower than the 8 mixing cycles, the last showed less variation between experiments, indicating greater consistency. This is crucial because homogeneity between the samples would translate into fewer errors and higher accuracy when they are used in HTS assays.

The final experiment assessed whether the cylindrical nozzle lead to a risk to cell survival and if the time between mixing and dispensing affected cell homogeneity across wells. The results, shown in Figure 4.7 and 4.12, indicated that the viability of

samples exposed to the cylindrical nozzle was similar to the control and the conical nozzle. Moreover, cell growth increased across the incubation days, suggesting that the cylindrical needle does not induce significant stress or apoptosis in cells. This contrasts with previous studies that indicate a smaller middle radius of the cylindrical nozzle creates higher stress and cell damage compared to the conical nozzle, resulting in lower viability [47, 48]. However, since only one experiment was conducted, further experiments are necessary to confirm these findings. Additionally, as mentioned earlier, the cylindrical nozzle did not improve droplet centralization and required higher dispensing control. Therefore, these findings suggest that the cylindrical nozzle may not offer an advantage over the conical nozzle for this workflow.

For samples dispensed four hours after mixing, significant differences were observed compared to immediate dispensing (see Figure 4.17). The CV increased to 16.61% after 6 hours of incubation, compared to 6.62% for the control. Analysis of cell distribution across wells (see Figure 4.18) showed that the control maintained homogeneity, while samples dispensed after four hours exhibited fewer cells in the initial wells. This could be attributed to cell sedimentation, where cells begin to settle after being in solution for four hours, leading to stress and potential cell death due to nutrient and oxygen deprivation, accumulation of metabolic waste, and contact inhibition [49]. But as previously mentioned, more experiments should be performed to prove the results found for this condition.

In summary, this study aimed to evaluate and optimize the BIO CELLX bioprinter for high-throughput applications by addressing four key research questions. The validation process identified several software and hardware issues, with significant improvements achieved through iterative testing and feedback, resulting in a functional workflow. Evaluation of the printer's features demonstrated accurate mixing and dispensing, with pH levels suitable for cell survival and droplet volume precision meeting technical requirements. However, issues like evaporation and condensation highlighted the need for controlled environmental conditions. Optimizing the dispensing process with different nozzle types showed improved droplet centralization using larger gauge nozzles. Cell viability studies indicated no cytotoxic effects, with high viability rates and consistent proliferation across different mixing cycles. Despite some variations, the overall findings suggest that the BIO CELLX bioprinter is a viable tool for high-throughput applications, although further testing needs to be conducted to acquire workflow reliability and replicates of some of the experiments are needed to confirm certain observations.

6
Conclusion

This study gives a comprehensive analysis on the workflow and functionalities of the prototype bioprinter developed by CELLINK, known as BIO CELLX. The aim was to evaluate its potential as a candidate or advancing 3D bioprinting to high-throughput levels. However, to be able to print in a 384-well plate while meeting all the requirements for HTS is a challenging task, demanding high precision and low error rates. This work focused on validating the BIO CELLX workflow to achieve full functionality, minimizing errors, and evaluating key features essential for printing small droplets, such as mixing efficiency, volume accuracy, and evaporation rates. Additionally, efforts were made to optimize dispensing parameters to achieve better droplet centralization while ensuring high cell viability and consistent cell homogeneity across prints.

After analyzing and discussing the results, it can be stated that a fully functional workflow has been achieved and validated, capable of completing all the steps necessary to create a 3D in vitro model. The final dispensed droplets exhibit high volume accuracy and well-mixed composition. Furthermore, it was found that using a 20G conical nozzle with customized dispensing parameters and performing 8 cell mixing cycles resulted in centralized droplets with high cell viability and consistent, homogeneous cell density distribution between samples.

Despite BIO CELLX's great potential to be considered a high-throughput bioprinter, there are areas that need improvement to fully realize this potential. Enhancing reliability, reducing printing times, and increasing control over temperature and humidity inside the bioprinter's compartment are critical areas for development. With these improvements from the prototype stage, there is no doubt that BIO CELLX could represent a significant advancement in the future of 3D bioprinting.

Bibliography

[1] Bon Kang Gu, Dong Jin Choi, Sang Jun Park, Min Sup Kim, Chang Mo Kang, and Chun-Ho Kim. 3-dimensional bioprinting for tissue engineering applications. *Biomaterials Research*, 20(1):1–12, 2016.

[2] Y. Xiang, K. Miller, J. Guan, W. Kiratitanaporn, M. Tang, and S. Chen. 3d bioprinting of complex tissues in vitro: State-of-the-art and future perspectives. *Archives of Toxicology*, 96(3):691–710, 2022.

[3] G. Gao, M. Ahn, W.-W. Cho, B.-S. Kim, and D.-W. Cho. 3d printing of pharmaceutical application: Drug screening and drug delivery. *Pharmaceutics*, 13(9):1373, 2021.

[4] L. M. Mayr and D. Bojanic. Novel trends in high-throughput screening. *Current Opinion in Pharmacology*, 9(5):580–588, 2009.

[5] M. R. Carvalho, D. Lima, R. L. Reis, J. M. Oliveira, and V. M. Correlo. Anticancer drug validation: The contribution of tissue engineered models. *Stem Cell Reviews and Reports*, 13(3):347–363, 2017.

[6] K. V. Kitaeva, C. S. Rutland, A. A. Rizvanov, and V. V. Solovyeva. Cell culture based in vitro test systems for anticancer drug screening. *Frontiers in Bioengineering and Biotechnology*, 8, 2020.

[7] C. Jensen and Y. Teng. Is it time to start transitioning from 2d to 3d cell culture? *Frontiers in Molecular Biosciences*, 7, 2020.

[8] L. P. Ferreira, V. M. Gaspar, and J. F. Mano. Design of spherically structured 3d in vitro tumor models - advances and prospects. *Acta Biomaterialia*, 75:11–34, 2018.

[9] T. S. Biju, V. V. Priya, and A. P. Francis. Role of three-dimensional cell culture in therapeutics and diagnostics: An updated review. *Drug Delivery and Translational Research*, 13(9):2239–2253, 2023.

[10] P. Bédard, S. Gauvin, K. Ferland, C. Caneparo, È. Pellerin, S. Chabaud, and S. Bolduc. Innovative human three-dimensional tissue-engineered models as an alternative to animal testing. *Bioengineering*, 7(3):115, 2020.

[11] O. Urzì, R. Gasparro, E. Costanzo, A. De Luca, G. Giavaresi, S. Fontana, and R. Alessandro. Three-dimensional cell cultures: The bridge between in vitro and in vivo models. *International Journal of Molecular Sciences*, 24(15):12046, 2023.

[12] Elisabete C. Costa, André F. Moreira, Duarte de Melo-Diogo, Vítor M. Gaspar, Marco P. Carvalho, and Ilídio J. Correia. 3d tumor spheroids: An overview on the tools and techniques used for their analysis. *Biotechnology Advances*, 34(8):1427–1441, 2016.

[13] Maddaly Ravi, V. Paramesh, S.R. Kaviya, E. Anuradha, and F.D. Paul Solomon. 3d cell culture systems: Advantages and applications. *Journal of Cellular Physiology*, 230(1):16–26, 2014.

[14] T.D. Ngo, A. Kashani, G. Imbalzano, K.T.Q. Nguyen, and D. Hui. Additive manufacturing (3d printing): A review of materials, methods, applications and challenges. *Composites Part B: Engineering*, 143:172–196, 2018.

[15] Ž.P. Kačarević, P.M. Rider, S. Alkildani, S. Retnasingh, R. Smeets, O. Jung, Z. Ivanišević, and M. Barbeck. An introduction to 3d bioprinting: Possibilities, challenges and future aspects. *Materials (Basel)*, 11(11):2199, 2018.

[16] B. Derby. Printing and prototyping of tissues and scaffolds. *Science*, 338:921–926, 2012.

[17] Y. He, Z. Gu, M. Xie, et al. Why choose 3d bioprinting? part ii: methods and bioprinters. *Bio-design and Manufacturing*, 3:1–4, 2020.

[18] T.G. Papaioannou, D. Manolesou, E. Dimakakos, G. Tsoucalas, M. Vavuranakis, and D. Tousoulis. 3d bioprinting methods and techniques: Applications on artificial blood vessel fabrication. *Acta Cardiologica Sinica*, 35(3):284–289, 2019.

[19] J.K. Placone and A.J. Engler. Recent advances in extrusion-based 3d printing for biomedical applications. *Advanced Healthcare Materials*, 7(8), 2017.

[20] M. Mobaraki et al. Bioinks and bioprinting: A focused review. *Bioprinting*, 18, 2020.

[21] A. Derossi et al. Extending the 3d food printing tests at high speed. material deposition and effect of non-printing movements on the final quality of printed structures. *Journal of Food Engineering*, 275:109865, 2020.

[22] E. Domínguez-Téllez, A. Serrano-Estrada, and J. B. Fuenmayor. A micro-extrusion 3d printing platform for fabrication of orodispersible printlets for pediatric use. *International Journal of Pharmaceutics*, 605:120854, 2021.

[23] A. Mazzocchi, S. Soker, and A. Skardal. 3d bioprinting for high-throughput screening: Drug screening, disease modeling, and precision medicine applications. *Applied Physics Reviews*, 6(1):011302, 2019.

[24] L. M. Mayr and D. Bojanic. Novel trends in high-throughput screening. *Current Opinion in Pharmacology*, 9(5):580–588, 2009.

[25] S. Markossian, A. Grossman, M. Arkin, et al. *Assay Guidance Manual*. Bethesda (MD): Eli Lilly & Company and the National Center for Advancing Translational Sciences, 2004.

[26] Bio cellx (2024). CELLINK. Available at: `https://www.cellink.com/bio-cellx/` (Accessed: 27 March 2024).

[27] S. Ramesh et al. Extrusion bioprinting: Recent progress, challenges, and future opportunities. *Bioprinting*, 21, 2021.

[28] A. Gangrade et al. Nanobioactive blood-derived shear-thinning biomaterial for tissue engineering applications. *Applied Materials Today*, 38:102250, 2024.

[29] S. Zhang and A. Khademhosseini. Advances in engineering hydrogels. *Science*, 356(6337), 2017.

[30] J. Malda et al. 25th anniversary article: Engineering hydrogels for biofabrication. *Advanced Materials*, 25(36):5011–5028, 2013.

[31] J. Stepanovska et al. Collagen bioinks for bioprinting: A systematic review of hydrogel properties, bioprinting parameters, protocols, and bioprinted structure characteristics. *Biomedicines*, 9(9):1137, 2021.

[32] E.E. Antoine, P.P. Vlachos, and M.N. Rylander. Review of collagen i hydrogels for bioengineered tissue microenvironments: Characterization of mechanics, structure, and transport. *Tissue Engineering Part B: Reviews*, 20(6):683–696, 2014.

[33] Telocol-10, solution, 10 mg/ml (2023). CELLINK. Available at: `https://www.cellink.com/product/telocol-10-solution-10-mg-ml/` (Accessed: 02 April 2024).

[34] M. Shayegan, T. Altindal, E. Kiefl, and N.R. Forde. Intact telopeptides enhance interactions between collagens. *Biophysical Journal*, 111(11):2404–2416, 2016.

[35] K.E. Fung, G. Su, C. Pehlke, S.M. Trier, K.W. Eliceiri, P.J. Keely, A. Friedl, and D.J. Beebe. Control of 3-dimensional collagen matrix polymerization for reproducible human mammary fibroblast cell culture in microfluidic devices. *Biomaterials*, 30(27):4833–4841, 2009.

[36] P. Nayak, V. Bentivoglio, M. Varani, and A. Signore. Three-dimensional in vitro tumor spheroid models for evaluation of anticancer therapy: Recent updates. *Cancers (Basel)*, 15(19):4846, 2023.

[37] I. Christodoulou, M. Goulielmaki, A. Kritikos, P. Zoumpourlis, G. Koliakos, and V. Zoumpourlis. Suitability of human mesenchymal stem cells derived from fetal umbilical cord (wharton's jelly) as an alternative in vitro model for acute drug toxicity screening. *Cells*, 11(7):1102, 2022.

[38] F.H. Chen et al. Mesenchymal stem cells. *Principles of Tissue Engineering*, pages 823–843, 2007.

[39] M. Klak, P. Kowalska, T. Dobrzański, G. Tymicki, P. Cywoniuk, M. Gomółka, K. Kosowska, T. Bryniarski, A. Berman, A. Dobrzyń, W. Sadowski, B. Górecki, and M. Wszoła. Bionic organs: Shear forces reduce pancreatic islet and mammalian cell viability during the process of 3d bioprinting. *Micromachines (Basel)*, 12(3):304, 2021.

[40] M. Flinck, S.H. Kramer, and S.F. Pedersen. Roles of ph in control of cell proliferation. *Acta Physiologica*, 223(3), 2018.

[41] S.O. Sarrigiannidis et al. A tough act to follow: Collagen hydrogel modifications to improve mechanical and growth factor loading capabilities. *Materials Today Bio*, 10:100098, 2021.

[42] M. Matamoros et al. Temperature and humidity pid controller for a bioprinter atmospheric enclosure system. *Micromachines*, 11(11):999, 2020.

[43] S. Naghieh and X. Chen. Printability–a key issue in extrusion-based bioprinting. *Journal of Pharmaceutical Analysis*, 11(5):564–579, 2021.

[44] R.C. Tolman. The effect of droplet size on surface tension. *The Journal of Chemical Physics*, 17(3):333–337, 1949.

[45] J. López-García et al. Hacat keratinocytes response on antimicrobial atelocollagen substrates: Extent of cytotoxicity, cell viability and proliferation. *Journal of Functional Biomaterials*, 5(2):43–57, 2014.

[46] T.M. Maul et al. Mechanical stimuli differentially control stem cell behavior: Morphology, proliferation, and differentiation. *Biomechanics and Modeling in Mechanobiology*, 10(6):939–953, 2011.

[47] E. Reina-Romo et al. Towards the experimentally-informed in silico nozzle design optimization for extrusion-based bioprinting of shear-thinning hydrogels. *Frontiers in Bioengineering and Biotechnology*, 9, 2021.

[48] R. Chand, B.S. Muhire, and S. Vijayavenkataraman. Computational fluid dynamics assessment of the effect of bioprinting parameters in extrusion bioprinting. *International Journal of Bioprinting*, 8(2):545, 2022.

[49] G.C. Cavalcante et al. A cell's fate: An overview of the molecular biology and genetics of apoptosis. *International Journal of Molecular Sciences*, 20(17):4133, 2019.

A

Appendix 1

A.1 Material unit and alginate capsule preparation

In order to assemble the Material Unit and prepare the alginate capsule for use in BIO CELLX, a detailed procedure must be followed to ensure proper functionality and accuracy.

First, all the necessary materials must be collected. This includes syringes, Luer locks, a micropipette, pipette tips, bioink and reagent capsules, various caps, a metal piston, a snap plunger with rubber sealing, a material unit holder, a nozzle insulator/aligner, a clean or new material unit, a 22G conical nozzle, and non-sterile 2% alginate. To start preparing the capsule, take a non-sterile 2% alginate syringe from the refrigerator. Hold the syringe upright and tap it to move any air bubbles to the top. Slide the plunger slightly to expel the air, then attach a Luer lock to the syringe tip and move the plunger until the alginate fills the Luer lock. Transfer the required volume of alginate plus an additional 10% to a 3 mL syringe, removing any air bubbles by rotating and tapping the syringe. Adjust the volume to 1.2 mL by extruding any excess material onto tissue paper. Connect the syringe to a clean bioink capsule with the white plunger at the bottom using a Luer lock, ensuring no bubbles are present in the capsule. If bubbles are detected, transfer the material back to the 3 mL syringe and repeat the process. Once the bioink capsule is bubble-free, attach it to the material unit.

Once the alginate capsule is prepared, proceed to the reagent capsule. Screw a clean reagent capsule onto the material unit. Set the volume of reagent (red-colored Milli-Q water) to 500 µL on the pipette and dispense it into the reagent capsule. Then, set the volume to 650 µL for cells (blue-colored Milli-Q water) on the pipette and dispense it into the cells chamber, ensuring the pipette touches the bottom side wall. Close each compartment with the corresponding cap.

To assemble the nozzle insulator/aligner into the material unit, insert it into the opening of the material support and screw the nozzle into the material unit. Introduce the material unit along with the nozzle insulator/aligner into the material unit holder, twisting the material unit until it is parallel to the material support and ensuring there are no gaps. Attach the cap protector to the nozzle.

Finally, take a snap plunger and a new rubber tip, avoiding direct contact with your fingers to prevent contamination. Attach the snap plunger and rubber together, then insert the snap plunger into the mixing chamber, aligning the grooves properly.

After completing these steps, the Material Unit is ready to be introduced into the material mixing station. This process ensures that the Material Unit and alginate capsule are properly prepared for use in the BIO CELLX, maintaining the integrity and accuracy of the dispensing and mixing procedures.

A.2 Material unit and capsules cleaning

Even though the material unit is intended to be a single-use product, due to its high cost, material units are cleaned and reused during validation work until they start to malfunction. However, a strict cleaning procedure must be followed to preserve the material unit as long as possible and ensure its correct performance.

Initially, the necessary materials are collected: a 5 mL syringe, Luer lock, metal piston, snap plunger with rubber sealing, screwdriver, air blow gun, and the used material unit. Additionally, it is important to ensure that the neutralizer, bioink capsule, nozzle, nozzle insulator/aligner, and cap protector are removed from the used material unit.

Once preparation is complete, the chambers can be cleaned. The same protocol can be followed for cleaning the extrusion chamber, cell chamber, and reagent chamber. First, position the slider valve hole to the required position depending on the chamber to be cleaned (see Fig. A.1). Fill a 5 mL syringe with water, attach a Luer lock, and connect it to the bottom of the material unit if cleaning the extrusion chamber, to the bioink position if cleaning the bioink chamber, or to the reagent position if cleaning the reagent chamber. For the cell chamber, simply add the water from the syringe into the chamber. Once the syringe is connected, inject water into the channel, moving the syringe and piston alternately. Disconnect the syringe, discard the water, and remove the piston. Dry the pertinent chamber with tissue or an air blow gun.

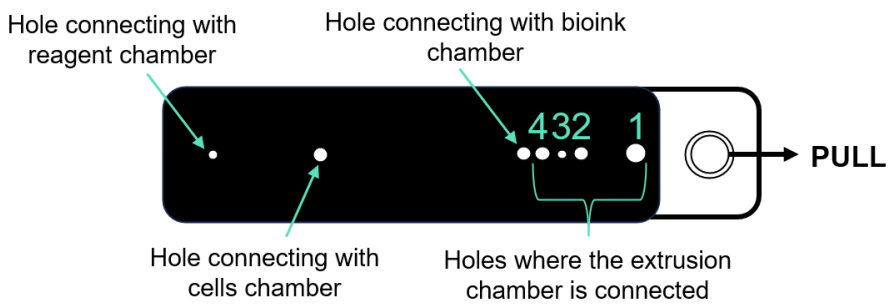

Figure A.1: Slider valve sketch showing the holes that connect to the extrusion chamber, bioink chamber, cell chamber, and reagent chamber.

For cleaning the reagent and bioink capsules, attach a water-filled syringe with a Luer lock to the reagent capsule with the white piston facing downward. Inject water and move the syringe plunger until the capsule is clean. Dry the capsule and piston with a tissue.

A.3 Viability studies for Experiment 1, 2, and 3

The results of Experiments 1, 2, and 3 are presented separately in this section.

For Experiment 1, the viabilities were as follows: On Day 1, the control showed a viability of 93.58% ± 1.04%, the 4 cell mixing cycles condition showed a viability of 92.15% ± 1.27%, and the 8 cell mixing cycles condition showed a viability of 94.85% ± 0.86%. On Day 4, the control showed a viability of 97.58% ± 0.43%, the 4 cell mixing cycles condition showed a viability of 96.79% ± 1.18%, and the 8 cell mixing cycles condition showed a viability of 96.43% ± 1.43%. On Day 7, the control showed a viability of 87.21% ± 5.34%, the 4 cell mixing cycles condition showed a viability of 89.99% ± 1.50%, and the 8 cell mixing cycles condition showed a viability of 92.21% ± 0.52% (see Fig. A.2A). The results for the live/dead ratio of Experiment 1 are shown in Figure A.2B. Additionally, images in Figure A.3 display live cells, dead cells, and total cells on Days 1, 4, and 7, observed using the fluorescent field in the microscope at 4x magnification. After performing unpaired t-tests and ordinary one-way ANOVA tests between conditions, no statistically significant differences were found, with all P-values exceeding 0.05.

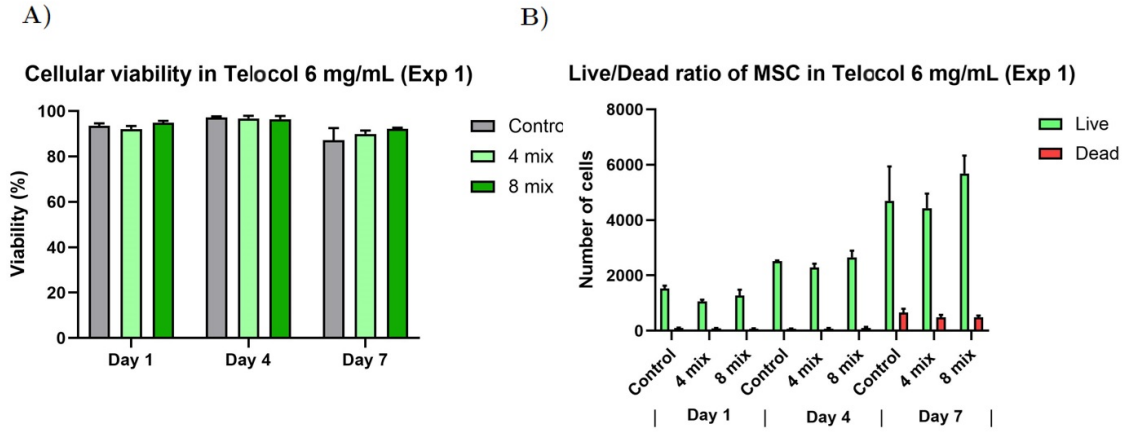

Figure A.2: Cell study results for Experiment 1 of cells embedded in TeloCol (6 mg/mL) droplets at day 1, 4 and 7 days after different nozzle conditions (conical or 8 cylindrical) compared to control (hand-dispensed). Data is shown as average ± standard deviation. Showing A) Viability percentage. B) Ratio of live cells (green) and dead cells (red).

For Experiment 2, the viabilities were as follows: On Day 1, the control showed a viability of 96.63% ± 0.92%, the 4 cell mixing cycles condition showed a viability

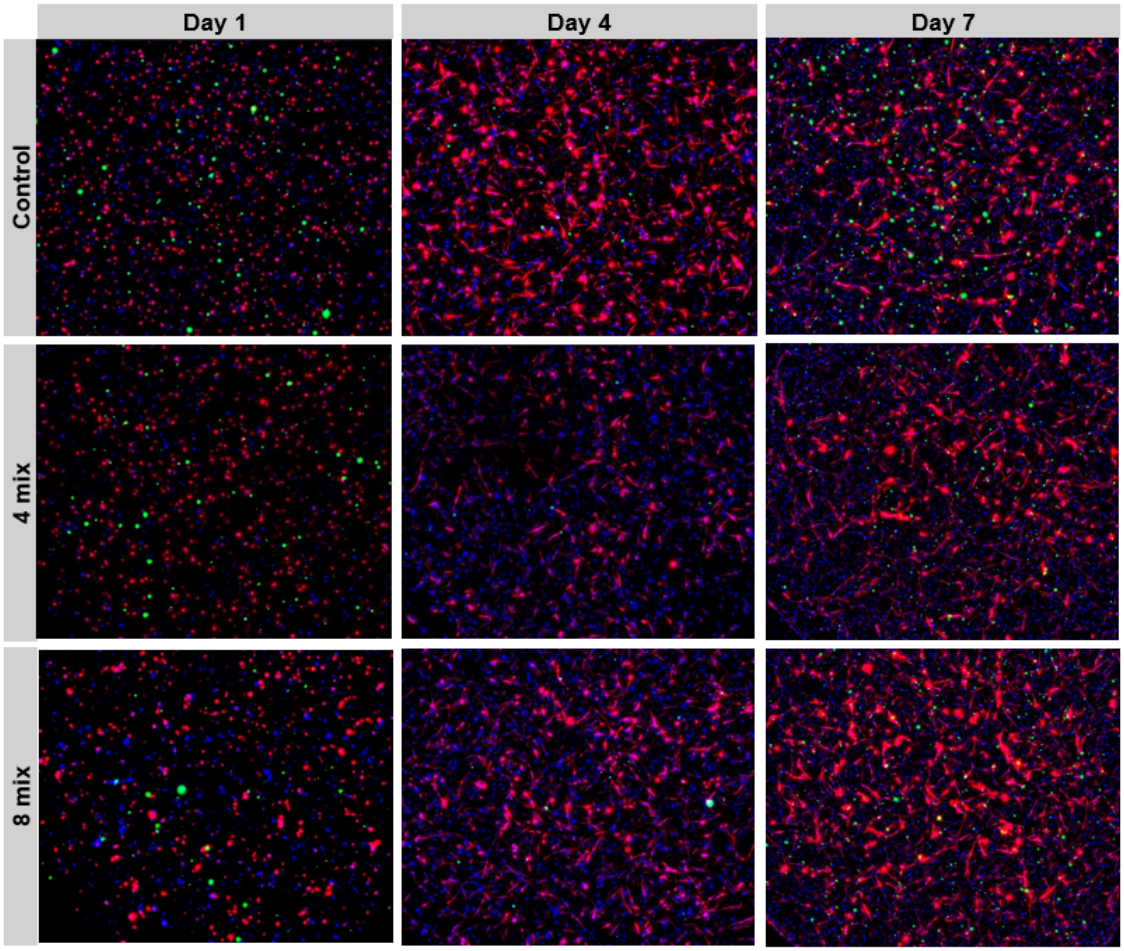

Figure A.3: Cell viability (live in red, dead in green, nucleus in blue) of printed droplets in Experiment 1 after mixing TeloCol and cells using the BIO CELLX or standard syringe to syringe mixing protocol. Representative pictures were taken after 1, 4 and 7 days for the BIO CELLX printed droplets and for the standard mixing protocol respectively. Pictures were obtained using the ECHO Revolve microscope with FITC and DAPI filters at 4X.

of 92.63% ± 2.20%, and the 8 cell mixing cycles condition showed a viability of 94.96% ± 1.62%. On Day 4, the control showed a viability of 94.71% ± 1.81%, the 4 cell mixing cycles condition showed a viability of 92.89% ± 2.95%, and the 8 cell mixing cycles condition showed a viability of 96.76% ± 0.59%. On Day 7, the control showed a viability of 87.82% ± 2.04%, the 4 cell mixing cycles condition showed a viability of 88.75% ± 3.65%, and the 8 cell mixing cycles condition showed a viability of 91.35% ± 0.50% (see Fig. A.4A). The results for the live/dead ratio of Experiment 2 are shown in Figure A.4B.

For the third and last experiment, the viabilities were as follows: On Day 1, the control showed a viability of 94.02% ± 0.72%, the 4 cell mixing cycles condition showed a viability of 93.66% ± 0.37%, and the 8 cell mixing cycles condition showed a viability of 91.62% ± 2.13%. On Day 4, the control showed a viability of 88.56% ±

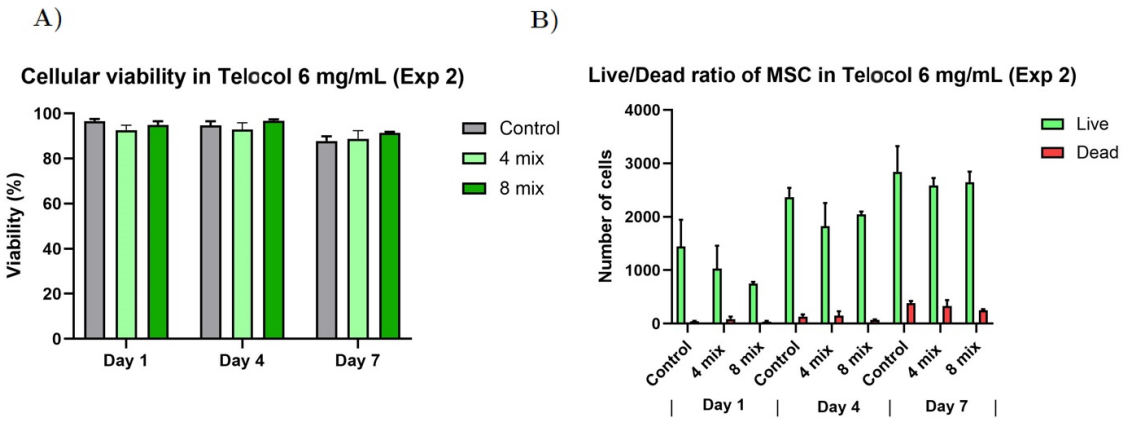

Figure A.4: Cell study results for Experiment 2 of cells embedded in TeloCol (6 mg/mL) droplets at day 1, 4 and 7 days after different nozzle conditions (conical or 8 cylindrical) compared to control (hand-dispensed). Data is shown as average ± standard deviation. Showing A) Viability percentage. B) Ratio of live cells (green) and dead cells (red).

0.99%, the 4 cell mixing cycles condition showed a viability of 95.46% ± 1.43%, and the 8 cell mixing cycles condition showed a viability of 96.12% ± 0.54%. On Day 7, the control showed a viability of 91.04% ± 1.47%, the 4 cell mixing cycles condition showed a viability of 93.82% ± 0.71%, and the 8 cell mixing cycles condition showed a viability of 93.38% ± 1.74% (see Fig. A.5A). The results for the live/dead ratio of Experiment 3 are shown in Figure A.5B. Furthermore, images in Figure A.6 display live cells, dead cells, and total cells on Days 1, 4, and 7, observed using the fluorescent field in the microscope at 4x magnification.

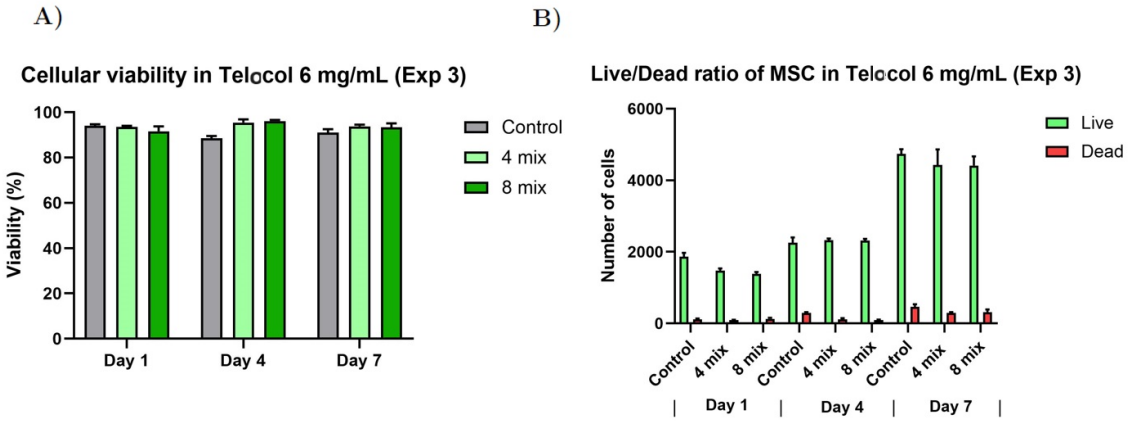

Figure A.5: Cell study results for Experiment 3 of cells embedded in TeloCol (6 mg/mL) droplets at day 1, 4 and 7 days after different nozzle conditions (conical or 8 cylindrical) compared to control (hand-dispensed). Data is shown as average ± standard deviation. Showing A) Viability percentage. B) Ratio of live cells (green) and dead cells (red).

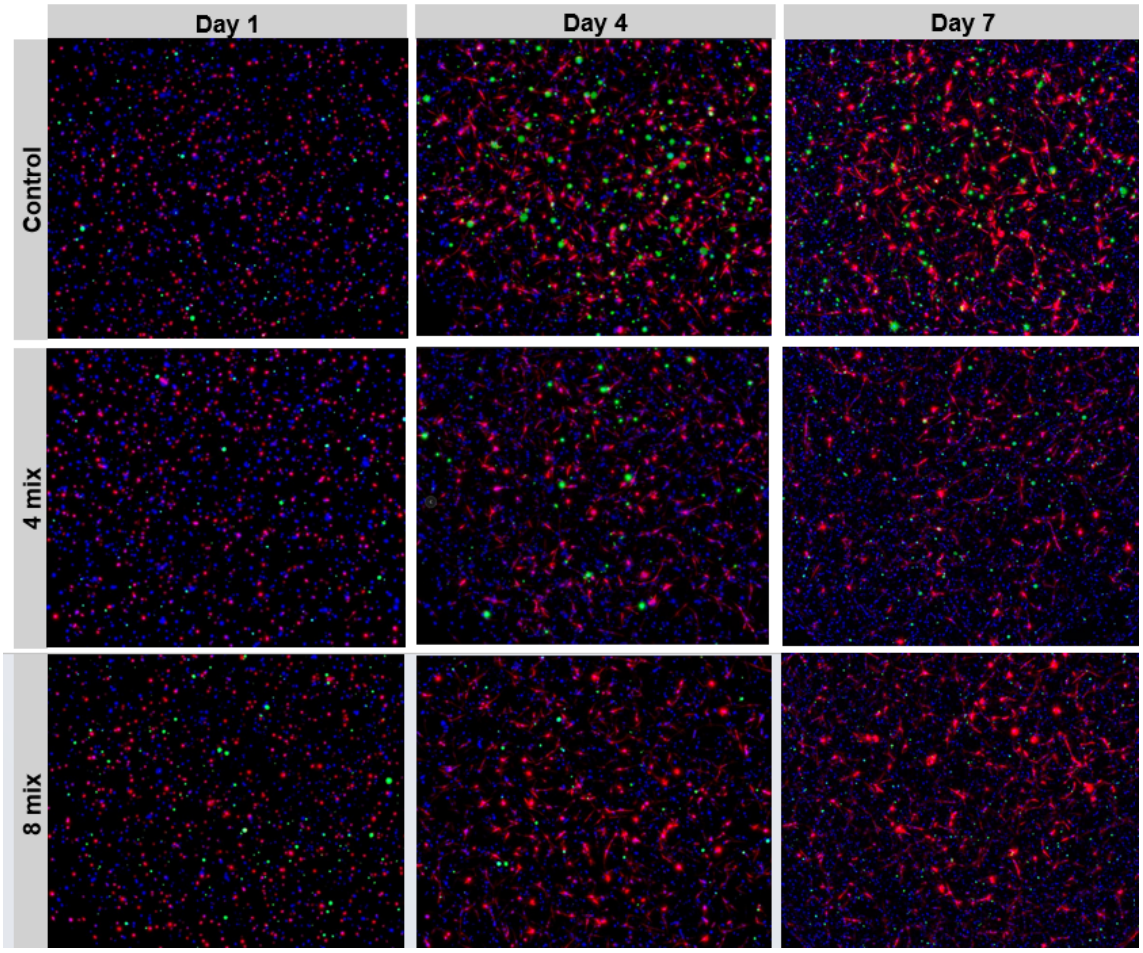

Figure A.6: Cell viability (live in red, dead in green, nucleus in blue) of printed droplets in Experiment 3 after mixing TeloCol and cells using the BIO CELLX or standard syringe to syringe mixing protocol. Representative pictures were taken after 1, 4 and 7 days for the BIO CELLX printed droplets and for the standard mixing protocol respectively. Pictures were obtained using the ECHO Revolve microscope with FITC and DAPI filters at 4X.

A.4 Homogeneity results for Experiment 1, 2, and 3

To ensure the reliability of the experiment and to determine which of the three incubation times produced the highest fluorescence activity and signal-to-noise ratio while maintaining a low standard deviation, the results were analyzed. As shown in Experiment 1 (Figure A.7, Figure A.8, and Figure A.9), the control parameters displayed the best results after 6 hours of incubation for all conditions tested. This pattern was also observed in Experiment 2 (Figure A.10, Figure A.11, and Figure A.12) and in Experiment 3 (Figure A.13 and Figure A.14).

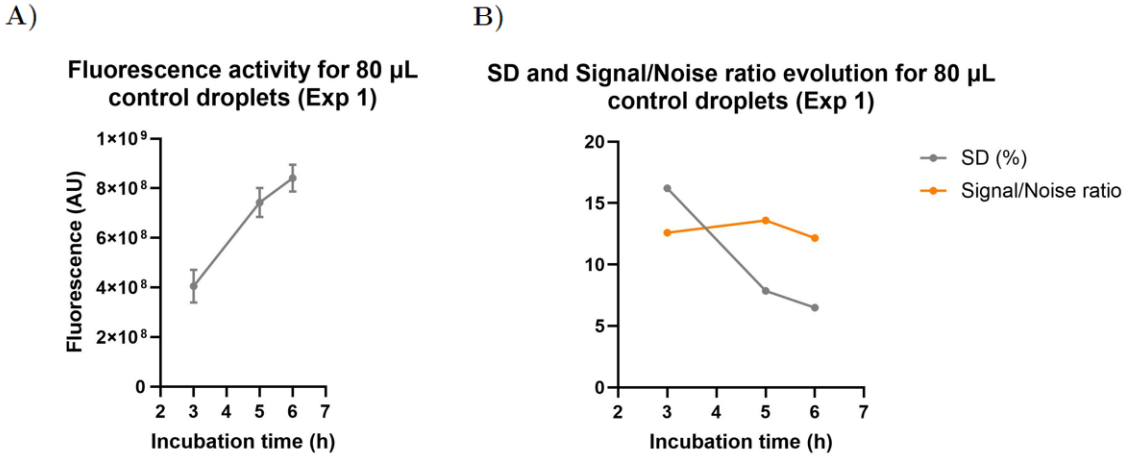

Figure A.7: Control parameters from homogeneity Experiment 1 in the control condition. A) Evolution of fluorescence activity expressed as relative fluorescence activity in arbitrary units (AU) over incubation time. B) Evolution of the standard deviation (SD) and the signal to noise ration over incubation time.

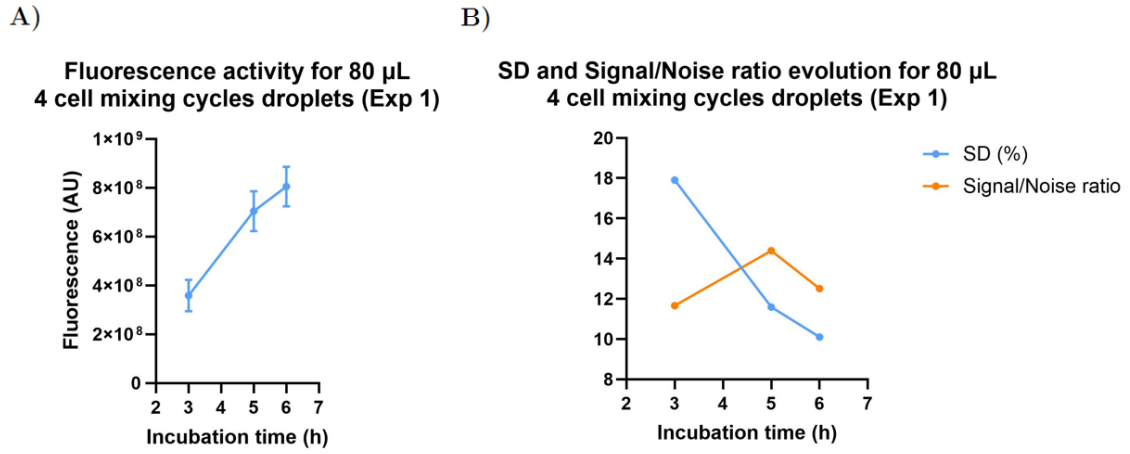

Figure A.8: Control parameters from homogeneity Experiment 1 in the 4 cell mixing cycles condition. A) Evolution of fluorescence activity expressed as relative fluorescence activity in arbitrary units (AU) over incubation time. B) Evolution of the standard deviation (SD) and the signal to noise ration over incubation time.

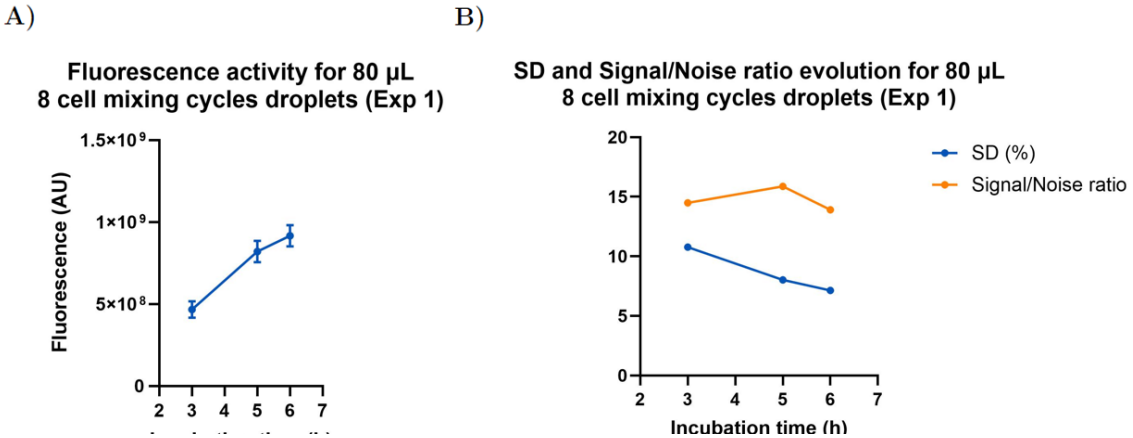

Figure A.9: Control parameters from homogeneity Experiment 1 in the 8 mixing cycles condition. A) Evolution of fluorescence activity expressed as relative fluorescence activity in arbitrary units (AU) over incubation time. B) Evolution of the standard deviation (SD) and the signal to noise ration over incubation time.

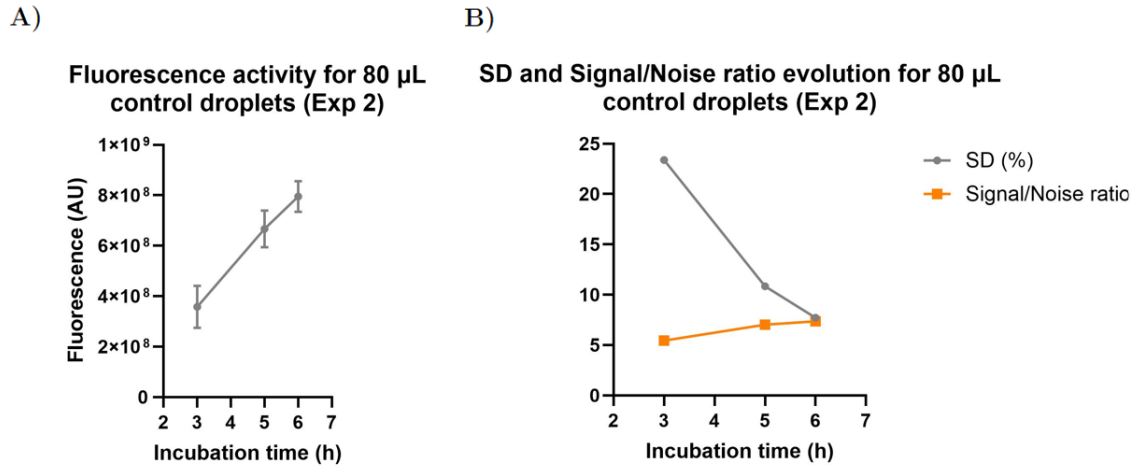

Figure A.10: Control parameters from homogeneity Experiment 2 in the control condition. A) Evolution of fluorescence activity expressed as relative fluorescence activity in arbitrary units (AU) over incubation time. B) Evolution of the standard deviation (SD) and the signal to noise ration over incubation time.

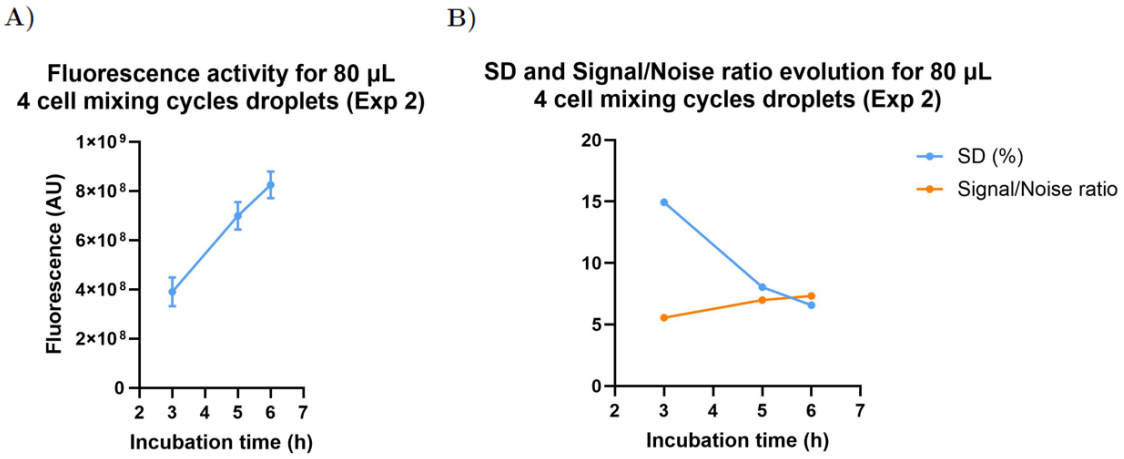

Figure A.11: Control parameters from homogeneity Experiment 2 in the 4 mixing cycles condition. A) Evolution of fluorescence activity expressed as relative fluorescence activity in arbitrary units (AU) over incubation time. B) Evolution of the standard deviation (SD) and the signal to noise ration over incubation time.

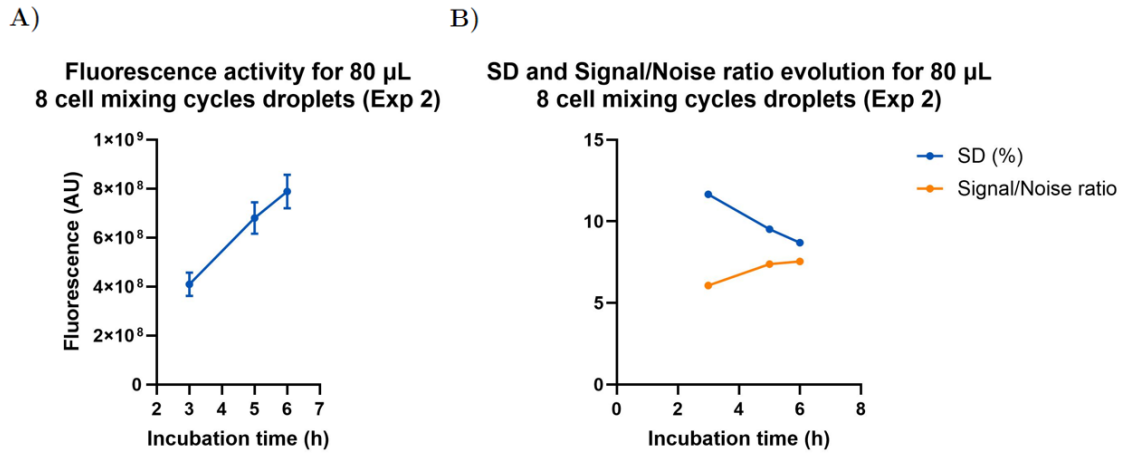

Figure A.12: Control parameters from homogeneity Experiment 2 in the 8 mixing cycles condition. A) Evolution of fluorescence activity expressed as relative fluorescence activity in arbitrary units (AU) over incubation time. B) Evolution of the standard deviation (SD) and the signal to noise ration over incubation time.

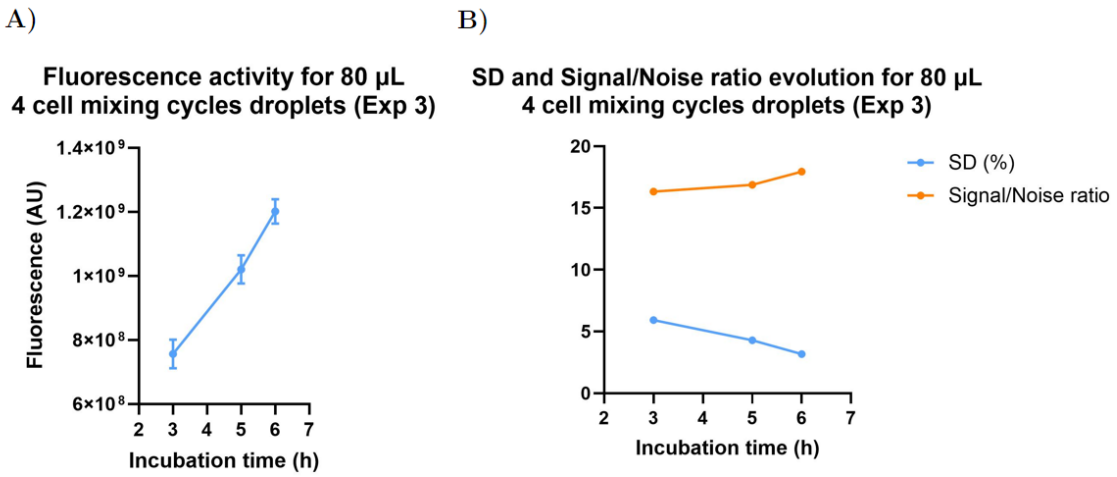

Figure A.13: Control parameters from homogeneity Experiment 3 in the 4 mixing cycles condition. A) Evolution of fluorescence activity expressed as relative fluorescence activity in arbitrary units (AU) over incubation time. B) Evolution of the standard deviation (SD) and the signal to noise ration over incubation time.

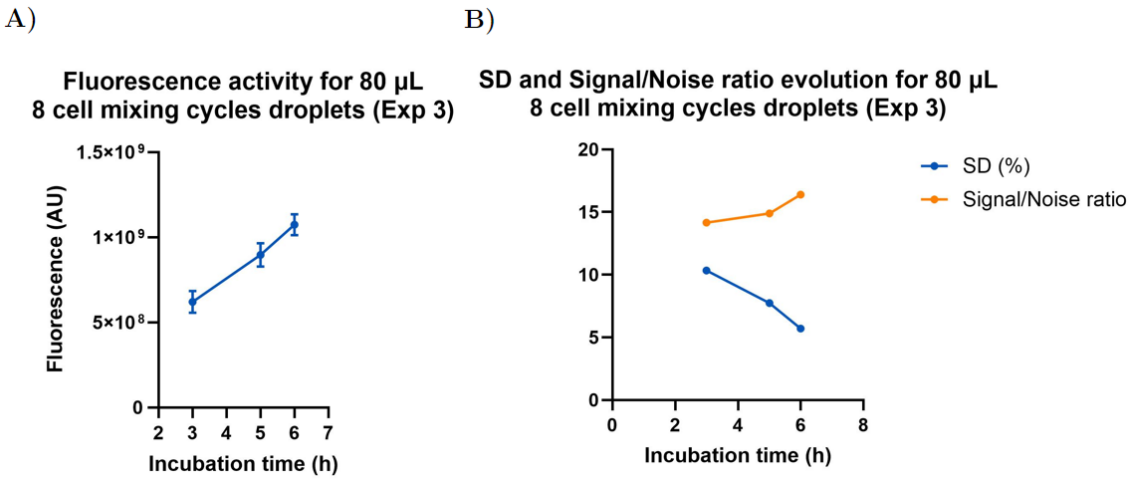

Figure A.14: Control parameters from homogeneity Experiment 3 in the 8 mixing cycles condition. A) Evolution of fluorescence activity expressed as relative fluorescence activity in arbitrary units (AU) over incubation time. B) Evolution of the standard deviation (SD) and the signal to noise ration over incubation time.

DEPARTMENT OF SOME SUBJECT OR TECHNOLOGY
CHALMERS UNIVERSITY OF TECHNOLOGY
Gothenburg, Sweden
www.chalmers.se

CHALMERS
UNIVERSITY OF TECHNOLOGY